GEORG-AUGUST-UNIVERSITÄT
GÖTTINGEN

Fakultät für
Physik

Master's Thesis

TCT Messungen am Diamanten für Spurdetektoren von Hochenergieexperimenten

TCT measurements with diamond for tracking detectors at high energy experiments

prepared by

Helge Christoph Beck

from Göttingen

at the II. Physikalischen Institut

Thesis number: II.Physik-UniGö-MSc-2015/05

Period: 1st April 2015 until 30th September 2015

First referee: Prof. Dr. Arnulf Quadt

Second referee: Priv.Doz. Dr. Jörn Große-Knetter

Contents

1. Introduction **1**

2. Interaction of particles with matter **3**

2.1. Cross section 3

2.2. Charged particles 3

2.3. Multiple scattering 6

2.4. Photons 6

2.4.1. Photoelectric effect 7

2.4.2. Compton scattering 7

2.4.3. Pair production and bremsstrahlung of electrons 7

2.5. Silicon detectors 8

2.6. Radiation damage 9

3. Diamond **11**

3.1. Synthesised Diamond 11

3.2. General properties compared to silicon 13

4. Transient current technique **17**

4.1. Signal creation and development 17

4.2. Theory 18

4.3. Example of a TCT measurement with scCVD diamond and silicon 20

4.4. Measurable properties 21

5. Measurement setup **23**

5.1. General set up 23

5.1.1. Radioactive source and vacuum chamber 24

5.1.2. Sensors 24

5.1.3. Readout electronics 25

5.1.4. Data acquisition 27

5.2. Problems 29
5.2.1. Breaking amplifiers 29
5.2.2. Noise 29

6. Analysis technique and results **31**
6.1. Measurements 31
6.1.1. General settings 31
6.1.2. Silicon diode data 31
6.1.3. Diamond data 32
6.2. Silicon diode 33
6.2.1. Averaging 33
6.2.2. Trigger ringing 36
6.2.3. Current calculation 38
6.2.4. Drift velocity and charge 41
6.2.5. Mobility 45
6.2.6. Trapping lifetime 46
6.2.7. CCD 47
6.2.8. Results and comparisons between data sets 49
6.3. Diamond 52
6.3.1. TCT voltage and current 52
6.3.2. CCD 54

7. Summary and outlook **57**

A. Data and Results **59**
A.1. Silicon diode 59
A.2. Diamond 76

1. Introduction

High energy physics experiments provide an inside look at the structure of the universe, the forces and especially the matter content of it. Since the second half of the 20$^{\text{th}}$ century more and more elementary particles and their interactions have been observed. The theory building for this is the standard model of particle physic (SM). It describes the electromagnetic, weak and strong interaction of fermions (spin one half particles) with mediating gauge bosons (spin one particles). The Higgs mechanism explains the origin of the mass of the particles.

But the SM is not complete. As astrophysics experiments show, the matter content of the universe is mostly unknown to us. The so called dark matter and dark energy are the largest part. The matter we observe and describe with the SM is only a small portion of the universe content. Other models like Supersymmetry try to solve this by adding more particles to the SM which have not been seen yet. The matter itself is not completely understood because matter and antimatter gets produced and destroyed pairwise but the universe consists only of matter. The CP violation, C being the charge conjugation and P the parity quantum number, found so far and explainable with the SM is not enough for this.

So clearly the SM is not the end. To test beyond SM (BSM) theories, new experiments have to be built and current ones upgraded. These experiments consist of particle sources and detectors for them. Common options for the first are accelerators as in the case of the Large Hadron Collider (LHC) at CERN or cosmic radiation and nuclear power plants. The detectors have to be chosen according to the particles. As the accelerators are stepped up in centre of mass energy (CME) and luminosity of the particle beams to get a chance to test the models the detectors have to bee improved, too. Because with higher CME particle tracks of interactions are more boosted and the distance between them is small. Better resolution is needed to distinguish them from each other. With higher luminosity the event rate is higher but also the pile up events meaning many hard interactions in one bunch crossing. This leads to a high occupancy of the detector resulting in reconstruction difficulties but also in high radiation damage especially in the inner detection layers. For these challenges, new radiation hard materials are needed and

one possible option is diamond.

With the chemical vapour deposition (CVD) technique synthesised diamond is available as poly-crystals (pCVD) and single crystals (scCVD). The later ones have a higher purity but they can not be produced on large scales and areas and are expensive. Because of that, pCVD diamonds are under test whether their performance is good enough for particle detection.

One method for testing detector properties is the transient current technique (TCT). With it, it is possible to measure the induced signal of drifting charge carriers in a material. From this, characteristic values of the material can be derived. In this thesis measurements with a silicon diode and a diamond are presented.

In the following chapters, first theoretical foundations are laid: Interaction of particles and matter will be discussed to lay the basics of particle detection 2, then the properties of diamond 3 and the measurement method TCT 4. The setup for the TCT measurement itself is described in 5 and the analysis of the measurements with its results in 6. A summary and an outlook are given in 7.

2. Interaction of particles with matter

The understanding of the interaction of particles with matter is the key point for designing a particle detector. Different materials have varying responses to particles passing trough, different particles interact differently, even the same particles with higher or lower energy behave differently. Particle detection relies on these interactions and tries to use them as well as possible but not all effects are non destructive, e.g. the material can get altered by the passage of a particle resulting in so called radiation damage.

In this chapter, basic interactions are discussed using the example of charged particles and photons basing on [1]. As an example for the theory, a silicon track detector is described. Also a short introduction is given to radiation damage in the last section.

2.1. Cross section

The cross section describes the probability of an interaction to take place. If a beam of particles hits a target, either another beam or a block of material, one can define the differential cross section $\mathrm{d}\sigma/\mathrm{d}\Omega$ as the average number of particles scattered in the angle $\mathrm{d}\Omega$ per unit time and per unit particle flux. The total cross section can be derived by integration over the angle $\mathrm{d}\Omega$. In general, this will depend on the particle energy.

2.2. Charged particles

The important force for interactions of charged particles with matter is the electromagnetic force. The particles scatter with the electrons or the nucleus via the coulomb potential. Basically particles excite or ionize atoms on their way and hence lose energy and get deflected from the original path. Most theories describing the interaction assume the electrons of the atoms to behave as free because the energy and the mass of the particles are much higher than the binding energy of the electron. If the particle itself is an electron other models have to be used, same for very heavy ions. To not get lost in different

small theories the concentration here is on heavy charged particles in the range of muons, protons and α-particles.

The mean energy loss per path length $-\left\langle \frac{\mathrm{d}E}{\mathrm{d}x} \right\rangle$ or stopping power for such particles can be calculated with the *Bethe-Bloch*-formula:

$$\left\langle \frac{\mathrm{d}E}{\mathrm{d}x} \right\rangle = -4N_A r_e^2 m_e c^2 z^2 \rho \frac{Z}{A} \frac{1}{\beta^2} \left[\frac{1}{2} \ln \left(\frac{2m_e c^2 \gamma^2 \beta^2}{I^2} T_{max} \right) - \beta^2 - \frac{\delta}{2} - \frac{C}{Z} \right] \tag{2.1}$$

N_A	Avogadro's number
r_e	classical electron radius
m_e	electron mass
c	vacuum speed of light
z	elementary charge of the particle
ρ	material density
Z	atomic number of the material
A	atomic weight of the material
β	relativistic velocity of the particle
γ	Lorentz factor
I	mean excitation potential
T_{max}	maximum energy transfer in one collision
δ	density correction
C	shell correction

Table 2.1.: Used symbols in equation (2.1).

An illustration of the formula can be found in figure 2.1 for muons in copper and the symbols in it are explained in table 2.1.

The maximum energy transfer T_{max} is achieved by a head on collision and the result of the kinematics with a particle of mass M is:

$$T_{max} = \frac{2m_e(c\beta\gamma)^2}{1 + 2m_e/M\sqrt{1+(\beta\gamma)^2} + (m_e/M)^2}.$$

The mean excitation potential is an average of the atomic levels. Since this is difficult to calculate empirical formulas are used but they do not display variations at closing atomic shells:

$$I = 12Z + 7\,\mathrm{eV} \qquad Z < 13$$
$$I = 9.67Z + 58.8Z^{-0.19}\,\mathrm{eV} \qquad Z \geq 13$$

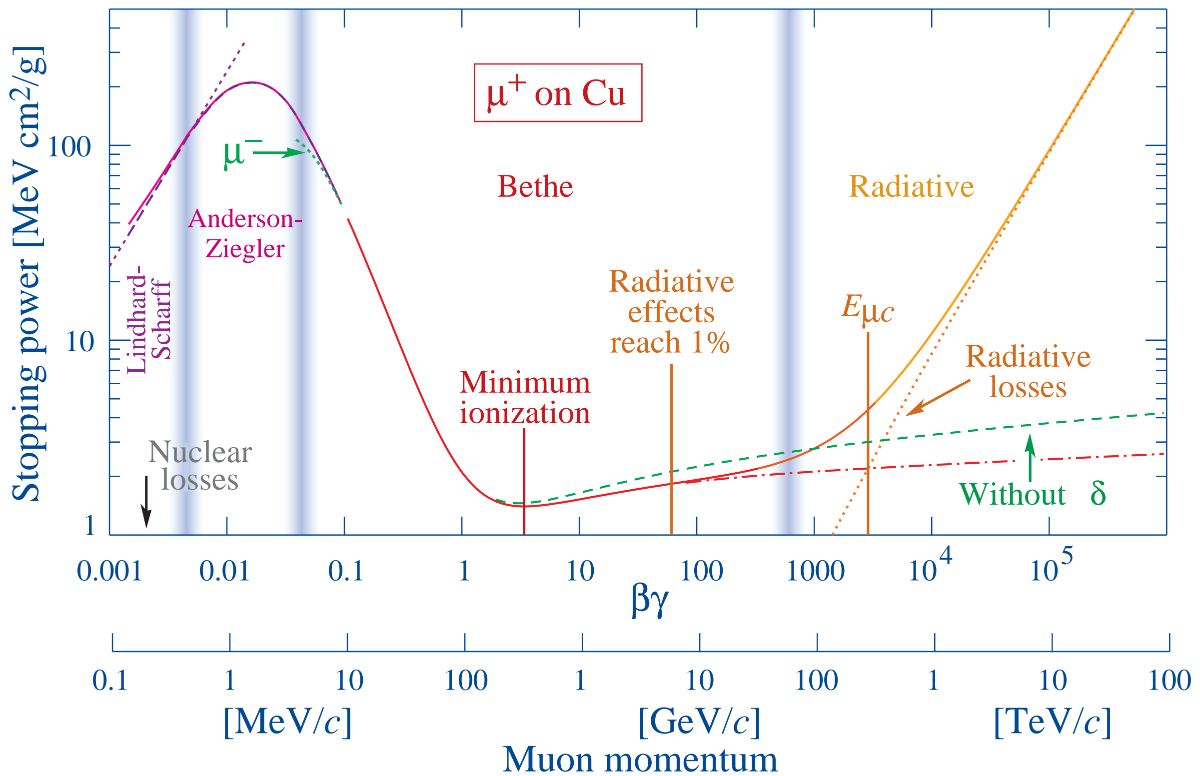

Figure 2.1.: Stopping power over a wide range of particle momentum and energy for muons in copper [2].

The density correction accounts for the polarization of the atoms along its path. Because of this, far away electrons are shielded from the field and add less to the energy loss. With higher particle velocity, the influence of electrons further away rises making this effect important for high energetic particles. The higher the density of the material the higher the polarization is and hence the name density correction.

The shell correction is a small contribution for low energies when the particle and electrons have comparable velocities and the electron thus can not be approximated as stationary. In this region the *Bethe-Bloch* formula breaks down.

For low particle energies the β^{-2} part is dominant. Different particles can be separated in this region with their specific energy loss because the slope is shifted for different masses. At a $\beta\gamma = 3 - 4$ particles reach a minimum energy loss and are therefore called minimum ionizing particles (m.i.p.). This loss is of about 2-3 MeV. With higher momentum the loss increases again slightly due to relativistic effects and reaches a plateau.

The energy loss of a particle in a material depends on the energy of the particle. A high energetic particle will lose only little energy at the beginning and the rate increases drastically after it is no more a m.i.p. and reaches the β^{-2} part. At this point the particle

gets stopped in the material within a short distance. Most energy is deposited near the stopping location. This behaviour is described by the *Bragg*-curve, figure 2.2.

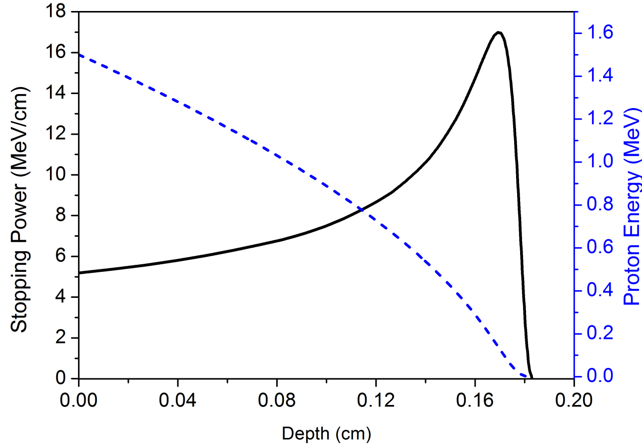

Figure 2.2.: Bragg curve and energy of protons in aluminium plasma [3].

2.3. Multiple scattering

Charged particles can also collide elastically with the nuclei instead of with the electrons via the Coulomb potential. This can be described with the Rutherford formula:

$$\frac{\mathrm{d}\sigma}{\mathrm{d}\Omega} = z_2^2 z_1^2 r_e^2 \frac{(m_e c/\beta p)^2}{4\sin^4(\theta/2)}.$$

Most collisions will have a small scattering angle θ due to the $\sin^{-4}(\theta/2)$ dependence. Many small deflections of the particle lead to a zigzag path and an overall scattering angle. Single scattering in very thin materials follows the Rutherford formula. A medium number of interactions can not be easily described but for many scatterings statistical methods can be applied. To discuss these is not aim of this thesis. Further information can be found here [1]

2.4. Photons

Since photons are electrically neutral they do not scatter inelastically with the electrons of the atoms as charged particles do. The main interactions in material for photons therefore are the photoelectric effect, Compton scattering and pair production. The first and last mentioned processes remove the interacting photon completely. The Compton

scattering changes its energy. The intensity I of a beam of photons exponentially decreases during the passage through the material from the starting intensity I_0 with an attenuation coefficient κ:

$$I(x) = I_0 \exp(-\kappa x)$$

2.4.1. Photoelectric effect

The absorption of a photon by an atomic electron and emission of that electron is known as the photoelectric effect. The electron energy is then the photon energy minus the binding energy. The electron has to be bound so the nucleus can take the recoil momentum for conservation of momentum.

The cross section for this process is high for low photon energies because the higher shell electrons have less binding energy. It decreases fast with higher photon energies except at energies where a new shell is available. There the cross section has a step. For MeV photons the cross section depends on the 4th or 5th power of the atomic number Z of the material.

2.4.2. Compton scattering

Compton scattering is the scattering of a photon with a free electron. In material this is given if the photon energy exceeds the binding energy. The photon transfers energy to the electron depending on the scattering angle. If the photon is back scattered the electron will receive the maximum amount of energy resulting in the Compton edge in the energy spectrum of the electron.

2.4.3. Pair production and bremsstrahlung of electrons

In this process the photon converts into an electron-positron pair. The threshold for this interaction is a bit higher than the sum of the masses of electron and positron because for energy conservation a third body has to take the recoil. In matter this is typically a nucleus.

This process is related to bremsstrahlung of an electron[1] in the vicinity of a nucleus, meaning radiation of photons from the electron. The coulomb field of the nucleus is needed for this reaction. The radiation length X_0 is the distance where the electron has only $1/e$ of his original energy. The cross section for pair production and bremsstrahlung

[1] or positron but for readability only electrons are mentioned

scale with Z^2 and the mean free path of pair production λ_{pair} and the radiation length are connected:

$$\lambda_{pair} \approx \frac{9}{7} X_0$$

A high energetic photon can result in an electron-photon shower in material generating electrons and positrons via pair production which again produce photons via bremsstrahlung. This will reduce the energy of the particles every interaction until the threshold for pair production is reached and other interactions get dominant.

In figure 2.3, the different interactions of photons with materials are shown for the example of lead. As explained above, the photoelectric effect is dominant for low energies, the Compton scattering for medium energies and the pair production above some MeV.

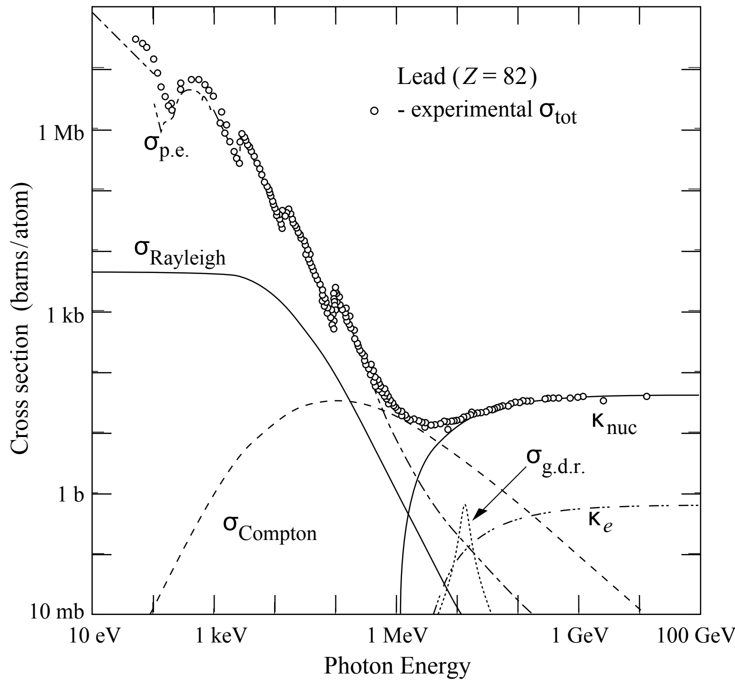

Figure 2.3.: Cross section of different photon interactions in lead [2].

2.5. Silicon detectors

At the moment silicon is the standard material for tracking detectors at high energy experiments. Also it has similar interactions with particles as diamond That is why it is here chosen as an example.

Silicon is a semiconductor which is described with the band model with a valence band and a conduction band separated by a gap. A passing through particle can ionize or

excite electrons into the conduction band leaving holes in the valence band. Both charge carriers can move independently in the material but they can recombine easily.

To prevent recombination and with it the loss of signal the silicon is doped differently. In the doped silicon, other atoms replace silicon atoms in the lattice introducing acceptors for electrons (p-type) or donors of additional electrons (n-type). Acceptor atoms have one electron less then silicon and donor atoms one more. If silicon is p-doped on the one side and n-doped on the other the extra electrons neutralize the holes where the zones of different doping meet. This results in a so called depletion zone. In it a electric field is formed by the atoms which are no longer neutral because of the exchange. This zone is in equilibrium with the rest of the material. An external bias voltage can be applied to widen the zone by shifting the equilibrium.

Electrons and holes created in the depletion zone drift away from each other because of the field and can hence induce a signal on the electrodes on the surface of the material, see section signal creation 4.1 in chapter 4. Normally, one aims for a complete depleted detector to get the most of the signal and a fast signal but there are other methods which only need partial depletion [4].

To measure the track of a particle, multiple layers of silicon detectors are needed, every one providing one point on the track. For this it is important that the passage through one detector does not alter the way of the particle in a major way. This can happen through the energy loss or multiple scattering. So the amount of interacting material has to be low without losing to much of the signal since less electron-hole pairs can be created.

2.6. Radiation damage

Lattice atoms can be displaced from their position by interacting particles. This creates defects in the material as vacancies and interstitials. A knocked off atom can produce more defects resulting in cluster defects if it has enough energy. The so induced modifications to the material result in changes of the signal of the particles to detect. The rest of the section will discuss changes in silicon because the behaviour is similar to diamond but longer under investigation [5, 6].

The defects in silicon create new energy levels between the valence and the conduction band. Levels in the middle of the band gap give rise to increased leakage current as thermal excitations get more likely. To reduce this effect, better cooling has to be used.

Trapping of electrons or holes can happen at levels near the bands. After some time the trapped charges are released but by then the signal collection can be finished without these charges. So the signal is decreased or even interferes with a following signal.

In silicon, the defects are mostly p-type resulting in a change of doping concentration. At high particle flux, an n-type sensor can even effectively be inverted to a p-type. With higher charge densities in the sensor a higher bias voltage has to be applied to completely deplete it. But they are limited by the design of the detector.

3. Diamond

Diamonds can not only be used for jewellery, they have also some very interesting physical properties. These make them an option for tracking detectors. In the ATLAS detector, the beam monitor detector consists already of diamond sensors and another tracking beam monitor has been installed with the IBL upgrade [7].

In this chapter, first the production of diamonds is explained and then their properties are compared to silicon, the standard tracking detector material.

3.1. Synthesised Diamond

The properties of natural diamonds are not reliable and they are not cheap either. They vary strongly in size and purity. Hence they are of no use for high precision applications. For this reason the industrial production of diamonds is growing and developing fast. One method to synthesise diamond is chemical vapour deposition (CVD) [8]. For this, pressures of few to tens of kilo pascals and temperatures of 700 to 1200 °C are needed which is orders of magnitude lower than natural genesis or other methods as the high pressure, high temperature (HPHT) one [9]. In this region, graphite is the stable conformation of carbon and not diamond. The trick to get diamond is the composition of the used gas in the process.

The gas is a mixture of hydrocarbon, e.g. methane, and hydrogen. The hydrogen leads to a sealed surface of hydrogen with five-member rings of carbon beneath. Hydrogen from the gas phase collides with the surface stripping some of the hydrogen away. This creates reaction possibilities for the hydrocarbon and its radicals to form in the next step a six carbon atoms ring, the diamond bulk. Graphite is also produced but the hydrogen etches it away in a higher rate than diamond.

The growth of diamond starts on a given substrate which determines already some properties of the diamond. At random positions the growth starts. These diamond seeds have the same orientation as the substrate at this place. Some orientations lead to a faster growth than others leading to bigger grains with this orientations. Single-crystal diamond (scCVD) can only be obtained by using another single-crystal diamond as substrate. So

all grains start with the same orientation and can form a single-crystal. For poly-crystals (pCVD) a silicon sample is sufficient.

The difference between pCVD and scCVD can be seen in figure 3.1. ScCVD diamonds have only impurities from the production e.g. resulting from contamination of the gas. But pCVD diamonds grow in different grains starting very fractioned at the seed surface and ending in bigger grains one the growth surface. Observations have been made that the boundaries of the big grains are more or less perpendicular to the growth surface. But even the bigger grains contain smaller structures [10].

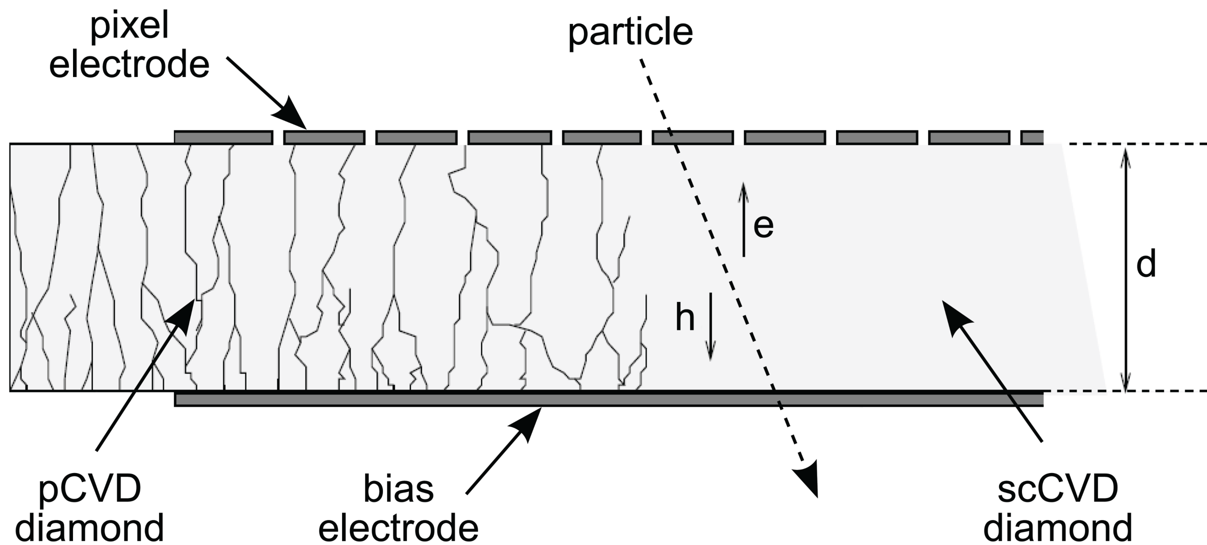

Figure 3.1.: Schematic of sc- and pCVD diamonds.

The charge collection distance CCD is an important property characterising the charge collection possibility of a material. It describes the mean distance electrons and holes drift apart before they are trapped. For a definition see equation (4.7). The scCVD diamonds have a higher CCD than the pCVD diamonds because of less impurities in the single-crystal. But with irradiation, the CCD decreases exponentially for both with the same damage constant [11]. So scCVD diamond has not a better response to high particle fluencies only a better starting point.

The production of scCVD is limited by the substrate size and the growth rate. With higher growth rates more impurities are created. This limits the efficient production of scCVD diamonds. The pCVD diamonds can have areas in the order of cm^2 and are cheaper. But they also have large amounts of impurities. So the tests of pCVD diamond for detector applications are important and can lead to larger instrumented areas with a reasonable expense if pCVD properties are good enough.

3.2. General properties compared to silicon

In table 3.1, some properties are listed for diamond and silicon which will be discussed in the following.

The comparison of diamond with silicon is a valid choice because the mechanism of signal creation by ionisation is the same for silicon and diamond. Their electron structure can be described with the band model of valence and conduction band. Also silicon is the standard material for tracking detectors at present. The production of silicon is industrially very well established with a high purity. Silicon itself has many options of how to build a detector whether it is a monolithic sensor with integrated readout electronic or a hybrid with separate sensor and read out. So in every application diamond has to compete with silicon.

Property	Diamond	Silicon
band gap [eV]	5.5	1.12
energy for a e/h-pair [eV]	13	3.6
radiation length [cm]	12.2	9.4
mean signal /µm [e]	36	89
intrinsic charge carrier density [cm^{-3}]	$< 10^3$	1.5×10^{10}
breakthrough field [V/cm]	10^7	3×10^5
resistivity [$\Omega\,\mathrm{cm}$]	$> 10^{11}$	2.3×10^5
dielectric constant	5.7	11.9
density [$\mathrm{g\,cm}^{-3}$]	3.52	2.33
dislocation energy [eV/Atom]	43	13-20

Table 3.1.: Properties of diamond and silicon [12].

Diamond is an isolator opposing to silicon which is a semi-conductor. This classification results from the high band gap for diamond of 5.5 eV and 1.12 eV for silicon. From this follows that a higher energy is needed to create an electron-hole pair in diamond which is 3.6 times higher than in silicon. This factor differs from a comparable factor between the band gaps. The circumstance that both materials feature indirect transitions between the bands is the reason. So more energy is needed for an additional phonon excitation. Also the resulting signal per micrometer material is less than half than in silicon.

The radiation length of diamond is 30% longer. So with the same detector thickness there is less energy deposited which means less signal creation again or the need for more material. That would lead to possible more multiple scattering and space requirements in an already dense packed region when considering multi-purpose detectors as ATLAS or CMS at CERN. But if the small signal is sufficient, less multiple scattering is achieved

with diamond with the same thickness of silicon.

Silicon detectors are used as a diode with a p-n- junction as described in section 2.5. They need a bias voltage to deplete the sensor of intrinsic charge carriers. The density of those in diamond is seven orders of magnitude lower, thus a depletion voltage is not necessary. But to collect the signal a voltage has to be applied to get reasonably short collection times by increasing the drift velocity and not relying on the diffusion process. See section 4.1 for signal development in matter.

The higher breakthrough field and resistivity of diamond allows to use high bias voltages. With high electric fields the drift velocity of the electrons and holes rises resulting in fast signals as needed for high particle flux environments.

But not only the creation of signal is important for a detector, also the noise or better the signal to noise ratio is the crucial property. The electrical noise induced from the sensor capacitance is lower for diamond because the dielectric constant is only half of silicon.

In addition to this, the high band gap for diamond is useful because thermal excitations are rare with so much energy. This leads to a small leakage current in comparison to silicon. The leakage current is poisson distributed and therefore the noise from this proportional to the square root of the current [6]. So a smaller leakage current means less noise. To reduce leakage current, cooling can be used so that thermal excitation is suppressed.

The thermal conductivity of diamond is high [8] so cooling is easier. Not the whole sensor has to be directly cooled. It could be sufficient to put the cooling next to the sensor because it can be better distributed. This reduces the cost and the space requirements of the detector.

For high luminosity experiments the particle flux is high near the interaction point. There are the tracking detectors placed for good position measurements of the different vertices. This requires materials that are radiation hard. Diamond has a higher dislocation energy for its atoms than silicon. Hence the damage done to the material from a particle in diamond should be less than in silicon. Especially consecutive damage from primary knock on atoms should be reduced.

One major issue is the trapping of charges in diamond i.e. electrons and holes get trapped in a long living state and do not contribute to the signal. Those states are introduced by radiation damage or intrinsic flaws in the lattice. Polycrystalline diamond has many grains and at their boundaries the lattice is disturbed because they do not line up properly. The property describing the mean distance which an electron and a hole separate by drift in an electrical field is the charge collection distance (CCD), definitions

see section 4.4. This distance is greatly influenced by the amount of traps.

All together diamond is an option for tracking detectors at high flux particle experiments. It has a smaller signal than silicon but with low noise this is not a problem. High particle rates can be observed because the charge collection in diamond is very fast.

4. Transient current technique

To determine charge collection properties of materials, the transient current technique (TCT) is a very powerful tool [6, 13, 14]. It can measure characteristics for electrons and holes independently by observing the signal of the charge carriers with time. The evolution of the signal takes a few nanoseconds. So a good time resolution is needed.

In this chapter, the general theory of TCT is discussed and how to infer from the measured pulse the physical properties of the sensor material. Example measurements for diamond and silicon are given.

4.1. Signal creation and development

After creation as discussed in chapter 2 charges move by diffusion or drift. Diffusion spreads the electrons and holes uniformly from their creation. Collisions reduce their energy until they recombine. The velocities are Maxwell distributed.

For drift an electrical field $\vec{E}$ is needed. The electrons and holes are accelerated along the field lines. Collisions with the atoms reduce the velocity and lead to a saturation velocity. The mean value of the velocity distribution is called drift velocity v_D. A useful property is the mobility μ of the charges which connects the field with the velocity:

$$\vec{v}_D = \mu \vec{E}. \tag{4.1}$$

The mobility depends only on the material not on the field. The mobility for electrons and holes can be different because electrons move in the conduction band and holes move by electrons jumping into them leaving a hole else where.

Even if drift is dominant diffusion is always happening at the same time. So a drifting charge cloud spreads also in other directions. This has more influence the longer the drift takes.

A signal is not only realised when the charges reach the electrodes but also during the drift. The moving charges q change the electrical field and induce a current on the

electrodes. This current is described by the *Shockley-Ramo* theorem [15, 16]:

$$I_{ind} = q \cdot \vec{E}_w(r(t)) \cdot \vec{v}_D(r(t)). \tag{4.2}$$

The electrical field is weighted with the applied voltage to the weighting field $\vec{E_w}$.

4.2. Theory

A schematic setup for a TCT measurement is given in figure 4.1. At the electrodes on the sensor a voltage is applied to collect the signal via drift of the charge carriers. From one side at one electrode the sensor is irradiated with laser pulses or α-particles. These create electron-hole pairs in the material but only up to a few micrometre depth then they are absorbed or stopped. For the setup with a laser, the wavelength has to be chosen appropriately to the material to get this kind of absorption and not produce a signal in the whole material. For diamond, α-particles are used because it has such a high band gap that laser excitation is difficult. The charge carriers are separated by the electrical field. Since they are near one electrode, the charges drifting to the electrode are sucked up almost immediately leaving only the carriers with the opposite electrical charge. Those drift to the other electrode through the whole sensor. The signal resulting from this drift is measured time resolved. So instead of a combination of both electron and hole signals one can observe one at a time. By irradiating the other side of the sensor or switching the sign of the voltage if this is possible for the sensor, e.g. not for silicon which needs depletion voltage, one can observe the other type of charges.

The amount of charges from the injection has to be small to not alter the electrical field. Also the rate of injections has to be low in order not to suffer from polarization effects. Those occur when charges get trapped and do not get released fast enough to not interfere with the next particle signal. This changes the electrical field because of the additional space charge.

Under the assumption of constant mobilities μ, the shape of the signal pulse can be calculated [14]. Trapping of charges is considered but the lifetime τ of the trapped state is assumed to be longer than the drift time t_D so de-trapping can be neglected.

With the configuration of planar electrodes one would expect a constant electrical field in the sensor but due to polarization there could be a constant space charge leading to a linear electrical field:

$$E(x) = E_0 - ax. \tag{4.3}$$

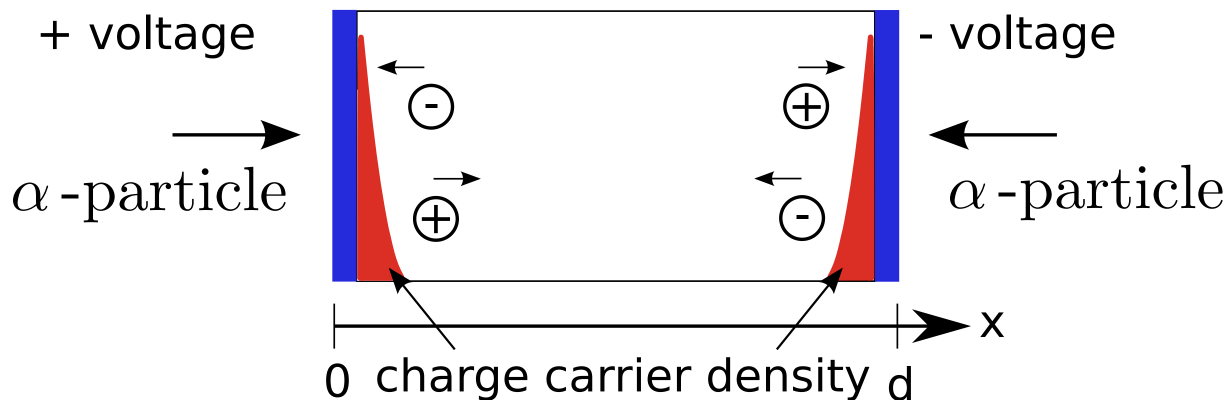

Figure 4.1.: Schematic of a TCT setup.

The cathode is at the origin of x and the other electrode at $x = F$ the detector thickness. The slope a is given by the space charge density N and the vacuum- and relative-permittivity ϵ_0 and ϵ_r, respectively:

$$a = \frac{eN}{\epsilon_0 \epsilon_r}.$$

With this field the equation of motion of the carriers from the definition of the mobility equation (4.1) can be solved:

$$x(t) = \frac{E_0}{a} \left(1 - \exp(-a\mu t)\right).$$

Trapping reduces over time the amount of charges Q drifting:

$$Q(t) = Q_0 \exp\left(-\frac{t}{\tau}\right).$$

To derive the current induced on the electrodes, the *Shockley-Ramo* theorem can be used, equation (4.2), with the last two formulas:

$$i(t) = \frac{Q(t)v(t)}{D} = \frac{Q_0 E_0 \mu}{D} \exp\left(\left(-a + \frac{1}{\mu\tau}\right)\mu t\right) \propto \exp(-ct). \tag{4.4}$$

The constant c can be obtained by fitting the measured current pulses. To calculate from that a, E_0, μ and τ more equations are needed.

One is the relation between the bias voltage U and the electrical field for a fully depleted sensor:

$$U = E_0 D - \frac{a}{2} D^2.$$

The second uses the fact that at $t = t_D$ the charges are at the other electrode at $x = D$:

$$x(t_D) = \frac{E_0}{a}\left(1 - \exp(-a\mu t)\right) = D.$$

That are not enough equations to solve this problem and additional input as measured values are needed. Another more empirical approach is described in section 4.4.

4.3. Example of a TCT measurement with scCVD diamond and silicon

TCT measurements have been done for scCVD diamond [13]. In figure 4.2, the pulse shapes of the current are displayed for different bias voltages from -40 V to -375 V for electrons and 70 V to 690 V for holes both from bottom to top peak in the graphs.

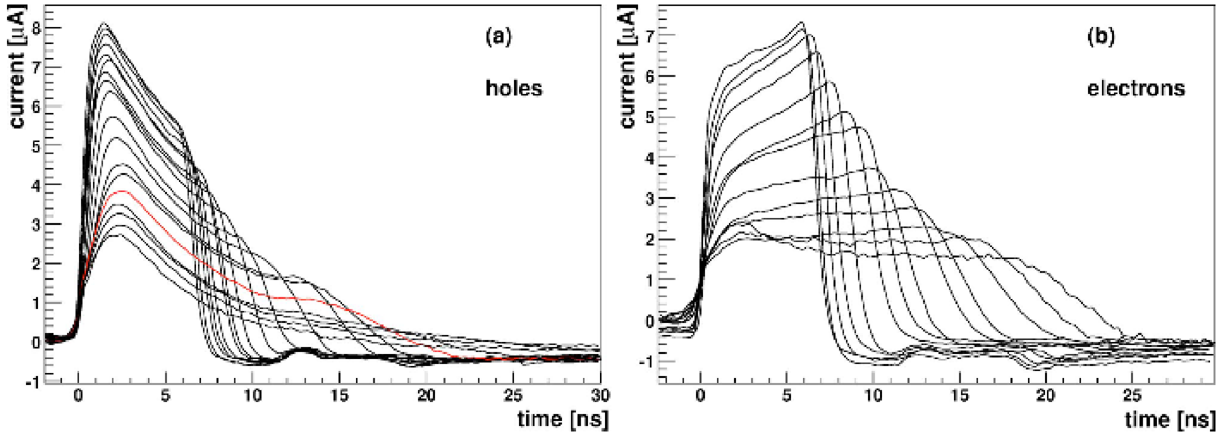

Figure 4.2.: Current pulse from scCVD diamond at different bias voltages for electrons and holes [13].

The pulse is separated in three parts. The first is the rising edge at the injection time. It is dominated by the readout electronics time constants.

Then the charge carriers drift and form the pulse. For electrons, an increase of the current with drift time can be observed and a decrease for holes. The effect for holes could be trapping of holes so the current gets reduced but in combination with the electron data this can not hold. A linear electrical field due to a negative space charge in the bulk explains the behaviour. While drifting to the opposite electrode, the field for holes reduces and electrons drift the other way. Resulting in higher or lower current, respectively.

The falling edge marks the arrival of the charge carriers except for holes below 80 V where the drift velocity is too slow because of the smaller field. The pulse is there dominated by diffusion. For higher bias voltages the holes reach the electrode.

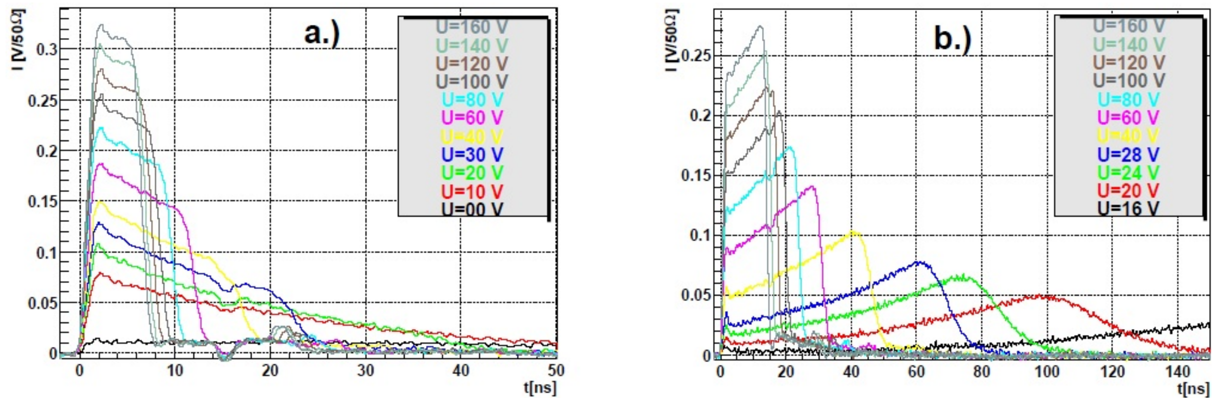

Figure 4.3.: Current pulse from a silicon diode, a) electrons, b) holes [17].

Silicon exhibits the same features as is shown in figure 4.3 [17]. For this measurements a $p^+ - n - n^+$ pad detector is used and a laser with a wavelength of 670 nm. The important difference in comparison to the diamond experiment is that the current for the electrons is falling during the pulse and for holes rising. The explanation for this is that the space charge in silicon has the opposite sign compared to diamond.

4.4. Measurable properties

From the pulse shape of the measured current one can derive different properties of the charge carriers in the material [13, 14]. The easiest one is the drift time t_D and with that the drift velocity v_D. The edges of the pulse define the start and the end of the drift and the difference is the drift time. But the start and end can be defined in different ways. At 50% of the pulse edge or even at 10% for the start. This induces a systematic uncertainty to the measurement. With the detector thickness D and the drift time t_D the mean drift velocity v_D of the pulse can be calculated:

$$v_D = \frac{D}{t_D}$$

It has been shown that the linear dependency of the drift velocity on the electrical field does not hold for typical detector voltages [13]. The reason is that the drift velocity saturates for this field due to the collisions of the charges with phonons. This formula is proposed instead:

$$v_D = \frac{\mu_0 E}{1 + \frac{\mu_0 E}{v_{sat}}}. \tag{4.5}$$

The parameter μ_0 is a low field mobility and v_{sat} the saturation velocity for electrons and holes, respectively.

To determine the trapping live time, the method of relative charge deficit can be used. For this the deposited charge $Q(U)$ is calculated by integrating the current pulse from its start to end. With the calculated mean drift velocity for each pulse the relative charge deficit can be written as:

$$\frac{Q_0 - Q(U)}{Q_0} \approx \frac{D}{2\tau}\frac{1}{v_D}. \tag{4.6}$$

By fitting the measured distribution $Q(v_D)$ with this formula one gets the lifetime of the charge carriers and the amount of charge without trapping Q_0.

An observable space charge can be a composition of many different traps and effects. But differentiation is not possible with TCT measurements so the measured effect is called an effective space charge. The effective space charge N_{eff} can be determined from the charge collection at different bias voltages, too. With increasing bias voltage the effect of the space charge is compensated. At a voltage U_C, the pulse of the holes in the example above exhibits a falling edge because of the arrival of the charge carriers. The depletion of the space charge is proportional to $\sqrt{U}$. The distribution of the collected charge corrected for the trapping shows a kink at U_C. The effective space charge depends on this voltage:

$$N_{eff} = \frac{2\epsilon_r\epsilon_0 U_C}{ed^2}.$$

The great advantage of TCT measurements is that electrons and holes can be observed independently. With the data for the mobility and the trapping lifetime one can calculate the charge collection distance CCD:

$$\mathrm{CCD} = (\mu_e\tau_e + \mu_h\tau_h)E. \tag{4.7}$$

It is the mean distance electrons and holes separate by drift before they are trapped.

5. Measurement setup

The TCT measurement setup is based on a system by Christoph Klein developed during his master thesis [18]. It was made for measurements with a laser and a radioactive source as injection mechanism for silicon and diamond samples.

In this thesis only the radioactive source is used. For this the set up was slightly modified. The setup itself and the changes and problems with it are described in this chapter.

5.1. General set up

For a TCT measurement three main parts are needed: An injection mechanism, the sensor to test, and a readout system. A picture of it is given in figure 5.1(a). First the general setup is described, then the main parts are explained in more detail.

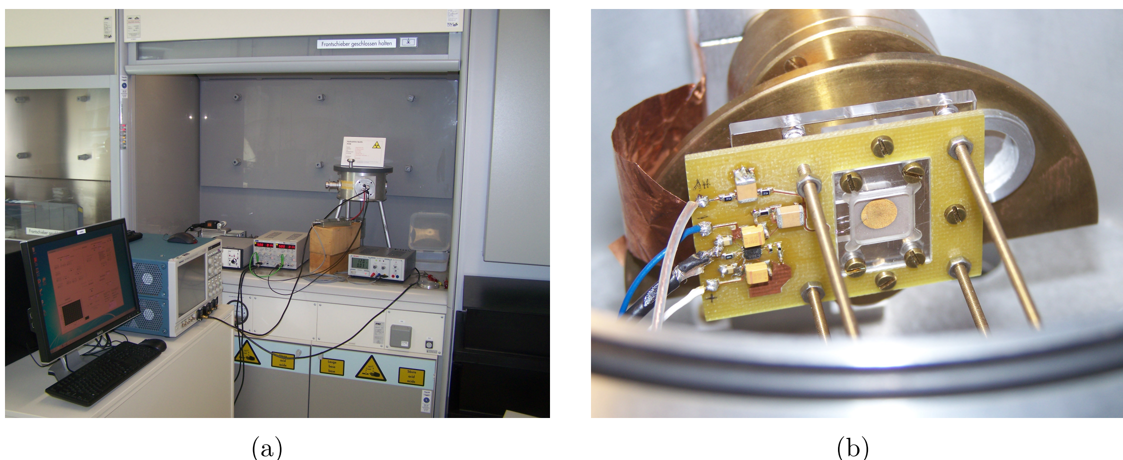

(a) (b)

Figure 5.1.: Pictures of the setup: in (a) the whole setup and in (b) the inside of the chamber in the top right of (a).

The central piece of the setup is the device under test, the sensor. It has two connections: one to the bias voltage supply and one to the readout. The bias voltage is supplied by an *iseg SHQ 122M* high voltage power supply which is able to provide positive and negative voltages. The readout system consists of an amplification circuit followed by an

oscilloscope. The oscilloscope is a *Tektronix DSA70804B* with a high bandwidth of 8 GHz. This is needed to resolve short pulses in the order of nanoseconds. For the amplification circuit a supply voltage of ± 5 V is needed and provided with a TTi PL303QMD-P dual power supply.

In addition to the operational amplifier on the circuit, an other amplifier can be used in between the circuit and the oscilloscope. It is a Kolter electronics VV1000-LC3E [19] with an amplification factor of 10.67 ± 0.02 [18] and low noise. A supply voltage of 12 V is needed and provided by a *Voltcraft VLP1202pro*.

The bias voltage supply and the oscilloscope are controlled and read out with a PC. For this a *LabWindows* program was written, see section 5.1.4.

5.1.1. Radioactive source and vacuum chamber

An ^{241}Am radioactive source is used to create electron hole pairs in the sensor near one electrode. It is an α-particle source with an α-energy of 5578.3 keV. To attenuate the energy an aluminium foil with a thickness of 10.9 µm is placed before it. This results in an energy behind the foil of roughly 4 MeV.

In air the α-particles are easily absorbed after a short distance. Therefore the radioactive source is mounted inside an air tight chamber with a pump connected to it. The sensor and the amplification circuit are also inside the chamber, see figure 5.1(b) for a picture. To protect the electronics against the radiation a plexiglass collimator is placed between the circuit and the source. Electric signals are routed in and out via four feed through's.

In front of the α-source a metal plate is installed with two holes. In on of them the aluminium foil is mounted. With a switch on the outside of the chamber the plate is turned to either block the particles, or let them through unchanged in energy or attenuated by the aluminium foil.

5.1.2. Sensors

Different sensors were investigated. One is a p-in-n silicon diode with the number 6137-03-16, see picture in figure 5.2. A SiO_2 layer protects the sensitive material on both sides. The diode is quadratic with a edge length of 6 mm. It has aluminium electrodes in the shape of hollow squares on either side. They have a side length of 3.5 mm and 3 mm for the p-side and the n-side, respectively. The central hole has an area of $1.5 \times 1.5\,\mathrm{mm}^2$. At the edges of the diode guard rings are implemented to protect against leakage current. The diode is 250 µm thick. It has a capacitance of (8.3 ± 0.2) pF [18]. With this diode

the setup is calibrated and checked as the properties of silicon are well known.

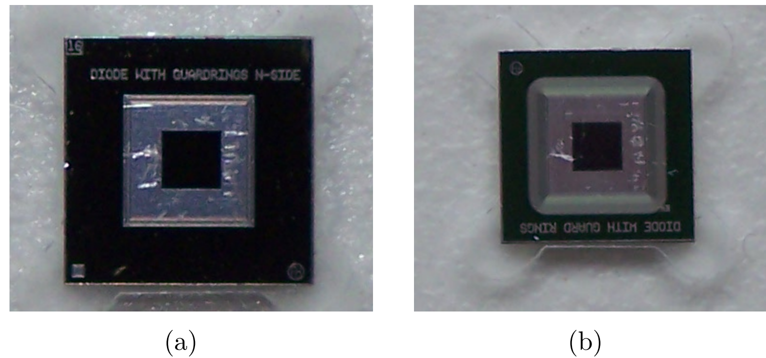

(a) (b)

Figure 5.2.: Pictures of the silicon diode, (a) n-side, (b) p-side.

The used diamond is a pCVD diamond with the number DB-DS-59, shown in figure 5.3. It is opaque indicating that it has been irradiated with high fluencies. Also the seed and growth side are clearly distinguishable, hinting that the sample was not polished after fabrication. It has a size of $10 \times 10\,\mathrm{mm}^2$ and a thickness of $400\,\mu\mathrm{m}$. The gold electrodes on both sides have a diameter of roughly 6 mm. The diamond has a capacitance of $C_d = (3.94 \pm 0.03)\,\mathrm{pF}$ [20].

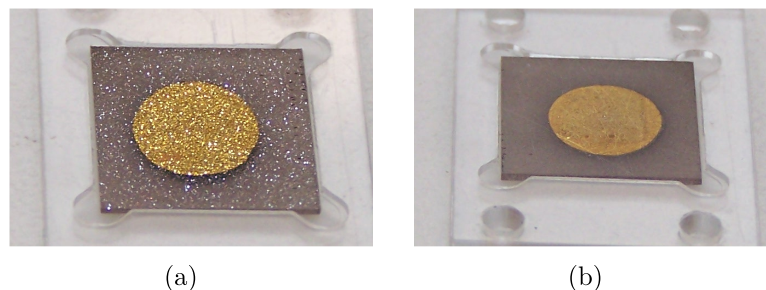

(a) (b)

Figure 5.3.: Pictures of the diamond sample DB-DS-59, (a) growth side, (b) substrate side.

5.1.3. Readout electronics

To measure fast signals with durations of some nanoseconds, a circuit board has been developed [18]. A short description is given here and then changes to the board during this master thesis are discussed.

In figure 5.4 a schematic of the electric circuit is shown. The central piece is the operational amplifier *AD8000* which has a high bandwidth of 600 MHz and a slew rate of 3700 V/µs in the used configuration. The amplifier is used non-inverting with a gain of

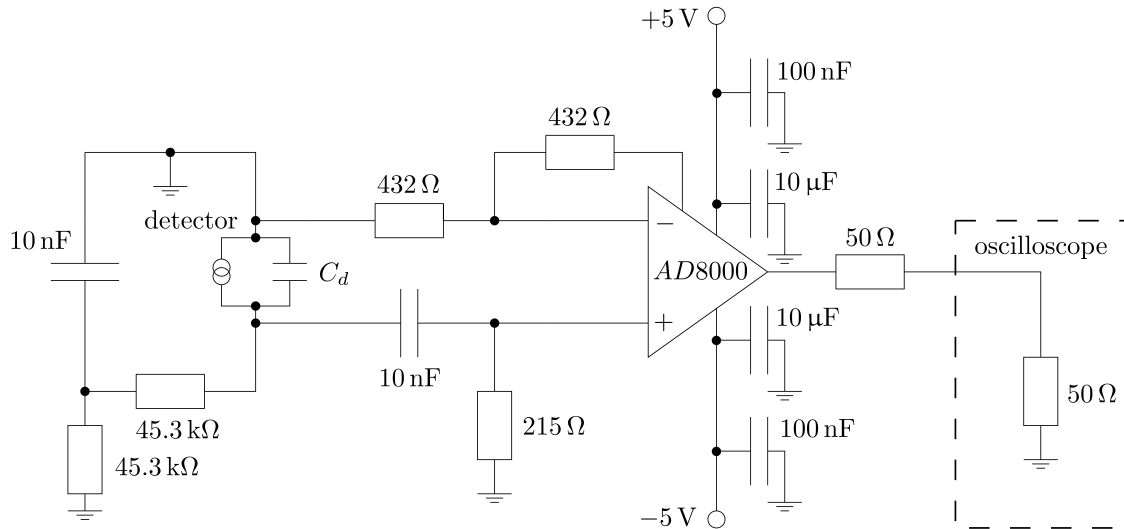

Figure 5.4.: Schematic of the electric circuit for the readout.

2 and an input resistor of 215 Ω. With the output resistor of 50 Ω only half of the signal is measured with the connected oscilloscope, resulting in a unity-gain. The resistor is important for the impedance matching to the oscilloscope input resistor which is needed for fast signals. The power supplies of ±5 V are bypassed with capacitors to reduce the base noise level.

The sensor is connected to a high voltage supply and to the amplifier. A capacitor blocks the high voltage from the sensor and only fast signals are let through to the amplifier.

All this is lain out on a PCB, for a picture see figure 5.5. This allows a compact build with small stray capacitances. The sensor is placed on the PCB in a cut-out and the connections to the circuit are made with wire bonds.

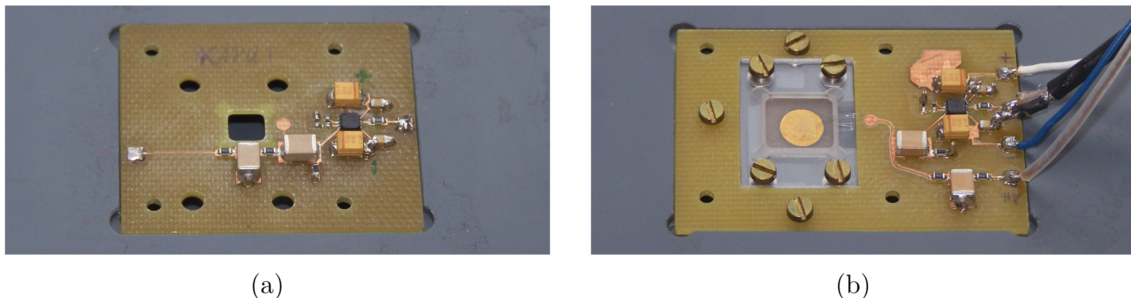

(a) (b)

Figure 5.5.: Picture of the readout electronic circuit before (a) and now (b).

Layout changes

The original design from [18] allows for measurements with a laser and a radioactive source. For the laser setup the high voltage supply for the sensor had to be on the opposite side of the side with the amplifier because of external limitations. For the setup with the α-source this is not optimal because all feed through's are positioned on one side of the source. This results in one wire crossing the chamber to the other side. In the new design all wire connections are on the side of the amplifier.

One important change for the usability of the setup is the new modular holder for the sensor. Previously there were two different PCBs for the diamond and the silicon diode because the holder was engraved into the PCB. Due to the different size of both samples two readout circuits were needed. One drawback of this is that the measurements of the samples could have systematic differences due to production of the circuit and the different parts used. The new design has a hole of $16 \times 22\,\mathrm{cm}^2$ at the former position of the sensor. In it a separate holder is placed for the samples. The holder is held in the PCB with three screws. With this change only one circuit is needed and for every sample a separate holder.

5.1.4. Data acquisition

The oscilloscope is read out via a GPIB interface. The user interface of the program for this is shown in figure 5.6. The programs main features are the configuration of the oscilloscope, the control of the bias voltage for the sensor and the reading and saving of the data from the oscilloscope. With these options measurements can be set up and conducted even by remote.

There are two action phases: first applying configurations, second measuring with the oscilloscope. These phases are strictly separated from each other, meaning that the configurations can not be changed during measurement.

Configurations

The configuration options for the oscilloscope are on the left side of the interface and the settings for the bias voltage supply on the right.

The standard configurations of an oscilloscope are available as selection of the trigger and the signal channel, the trigger level and the scale of the axis.

The bias voltage can be set for a single measurement but also for a series of measurements. Therefore a start and and end value can be chosen and the increment of the voltage between two measurements.

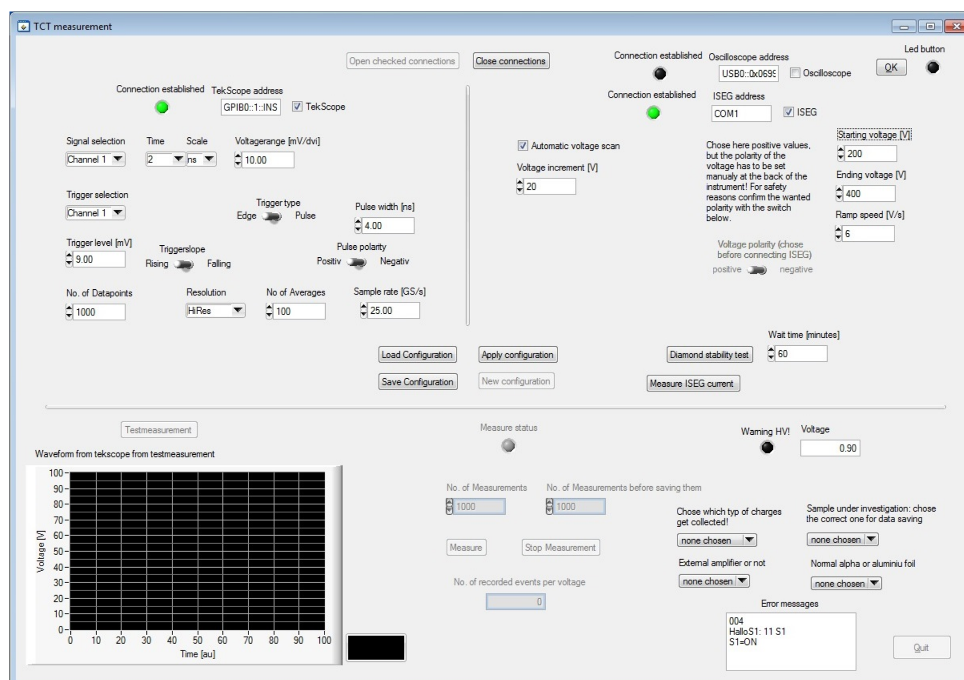

Figure 5.6.: User interface of the program for the data acquisition.

After a configuration is applied a measurement can be started.

Measurement

For the measurement there are only two options. How many events will be recorded and after how many events in the memory they get saved to disc. The later one is important to take fast data because the event rate is higher than the writing of events to disc. It is not optimal to write after every event but also not to wait for the final event.

Three button are available: One to start the measurement, one to stop it, and one to display the current event on the oscilloscope in the graph panel on the left side.

A measurement consists of applying a bias voltage, acquiring the chosen number of event from the oscilloscope and saving them. Normally a bias voltage range is specified so that multiple measurements are chained without further interactions with the program.

With the data also the chosen configurations and informations about the measurement are saved.

5.2. Problems

5.2.1. Breaking amplifiers

The original setup was partially broken at the start of this thesis. So only one PCB was left functioning. With this it was possible to take data with the silicon diode. But the amplifier on it broke while measuring with the diamond.

To find the reason for the breakdown, the stability of the diamond under high voltages up to 500 V was checked. A breakthrough of the diamond causes high currents which leads to a failure of the amplifier. For the measurement an addition to the program. It applies a voltage for a given time and measures the current every minute. The voltage range for the measurement is 100 V to 450 V and -100 V to -450 V in 50 V steps. Each voltage is applied for 60 minutes. The measurement does not show a breakdown of the diamond for bias voltages up to 450 V.

An other possibility for the breaking of the amplifier is that the heat from the amplifier is not dispersed fast enough, because there is not enough air in the chamber. To prevent an overheating a copper foil was attached to the backside of the PCB and connected to the chamber wall. There was not enough time to implement a measurement of the temperature in the chamber during the data taking. So this option remains unchecked.

The amplifier could not be replaced on the existing board. So a new board was designed with the modifications as described above in section 5.1.3. One amplifier broke again but with the latest board measurements for the silicon diode and the diamond were conducted.

5.2.2. Noise

During the last measurements with the diamond noise was observed with an amplitude of roughly 40 mV. The amplitude from the diamond signal is only about 14 mV. So a measurement was not possible. This noise was most probably not observed for the silicon diode because the signal is much higher from silicon and the trigger levels, too.

The vacuum pump, which was running during the measurements, was identified as the source for the noise. To test whether the pressure in the chamber is stable over time when the pump is switched off, the electron signal in diamond is measured with a bias voltage of 300 V three times in intervals of roughly an hour. The pump was on for five minutes before the first measurement. Since this was done on a Friday the chamber was left pressurized over the weekend. On the following Monday two measurements were done with the same settings as before without turning on the pump again. The external amplifier is used for these measurements.

This indirect test is the easiest option because there is no direct measurement of the pressure available. If air would leak into the chamber the amplitude of the signal should decrease with time because the α-particles lose energy to the air. Even the observation of no signal after some time would be possible.

In figure 5.7 the measured TCT signals are displayed and the mean difference in the signal region from each measurement to the first one after the pump was turned off. For every measurement 1000 events are averaged with the analysis program described later in chapter 6.

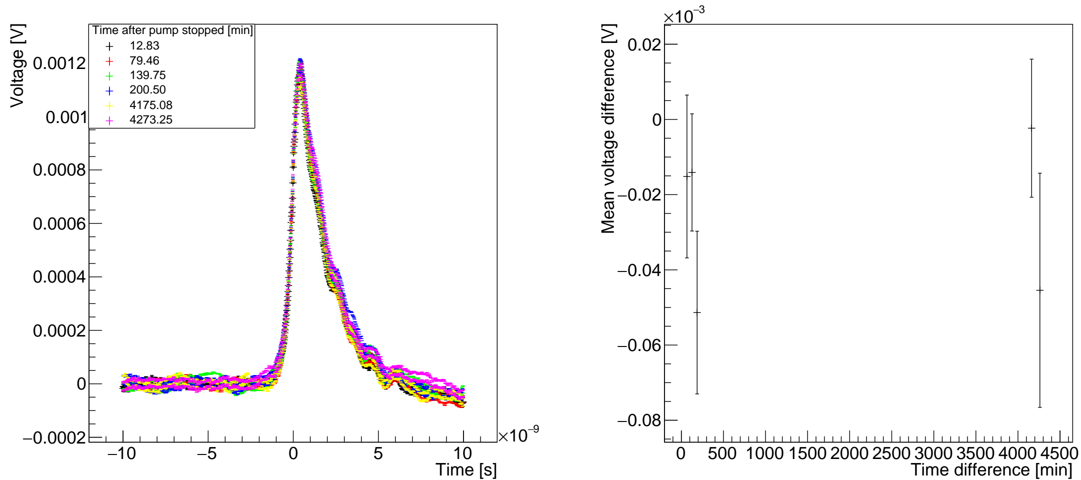

(a) TCT voltage pulses for the different measurement times.

(b) Mean difference in the signal region of each measurement to the first one.

Figure 5.7.: Voltage plots for the pressure stability test.

The only measurements showing a significant difference to the first measurement are the last measurement from Friday and the last from Monday which were made roughly 200 minutes and 71 hours respectively after the pump stopped. But the mean difference is only 50 µV which corresponds to a relative change to the amplitude of roughly 5 %. The first measurement on Monday is completely consistent with the first one. So despite some fluctuations the pressure in the chamber is stable over a long time period of days which is much longer than the time to measure one data set of roughly an hour.

6. Analysis technique and results

For the analysis of the data from the silicon diode and the diamond a *root* program is used. The theory of the analysis is described in chapter 4. In this chapter the different measurements and steps taken in the program are described. After that the results for the silicon diode and the diamond are discussed.

6.1. Measurements

Over the time of this thesis many measurements have been taken. As described previously the setup broke several times. From those runs the data is used to improve the analysis program and further data taking. The data used for the final analysis presented in this chapter is taken with the latest functioning setup. It contains complete measurements for the silicon diode and the diamond. The different settings for these data sets are presented here.

6.1.1. General settings

For all measurements an edge trigger on the signal is used with the matching falling or rising edge setting. The trigger point is in the centre of the time axis at 0 s. The resolution of the oscilloscope is set to at least 0.4 ns/point. Always 1000 events are recorded per bias voltage.

6.1.2. Silicon diode data

The p-side of the diode is bonded to the readout and the n-side to ground. The α-source faces the n-side for hole measurements and the p-side for electron measurements. For reverse biasing negative voltages are used.

Measurements were made at various distances between source and sample to test if the residual air in the chamber has a significant influence on the energy of the α-particles.

In the following table 6.1 the data sets are ordered by distances. The measurements are also classified by the usage of the external amplifier or not and the energy of the

Set	Position [mm]	Charge type	Ext. amplifier	Al foil	bias voltage U [V]	ΔU [V]
1.1	23.67	e	no	no	-50 to -140	10
1.2	23.67	e	no	yes	-60 to -140	10
2.1	25.18	e	no	no	-50 to -140	10
2.2	25.18	e	yes	no	-30 to -140	10
2.3	25.18	e	yes	yes	-50 to -140	10
3.1	28.25	e	yes	no	-30 to -140	10
3.2	28.25	e	yes	yes	-40 to -140	10
3.3	28.25	e	no	no	-50 to -140	10
3.4	28.25	e	no	yes	-50 to -140	10
4.1	27.78	h	no	no	-95 to -140	5
4.2	27.78	h	no	yes	-100 to -140	5
4.3	27.78	h	yes	no	-90 to -140	5
4.4	27.78	h	yes	yes	-100 to -140	5
5.1	26.17	h	yes	no	-90 to -140	10
5.2	26.17	h	yes	yes	-90 to -140	10
5.3	26.17	h	no	no	-90 to -140	10
5.4	26.17	h	no	yes	-100 to -140	10

Table 6.1.: Data sets for the silicon diode.

α-particles.

Electron signals can be observed for bias voltages larger than -10 V and holes signal for bias voltages larger than -90 V. The peak of the signal for these minimum bias voltages is only slightly above the noise background. Hence for the measurements higher voltages are chosen as start values. If the energy of the α-particles is reduced with the aluminium foil the signal amplitude is in general smaller which demands lower trigger levels and higher starting bias voltages. The bias voltage of -140 V is chosen as the end of the measurements to prevent breakdown of the diode at higher voltages.

The main data sets for the analysis of the silicon data are the 3.x and the 4.x because they have all combinations for electron and hole signal at roughly the same distance to the source. The slight difference is due to mispositioning after the turning of the PCB for the hole data. The other data sets are used to compare the different distances.

6.1.3. Diamond data

The growth side of the diamond is bonded to the ground of the circuit and faces the radioactive source. For positive bias voltages the drift of electrons is observed and for negative voltages the one of holes.

Neither electron nor hole signal could be observed without the external amplifier. There-

fore it has to be used for all measurements. No data set is recorded for the attenuated α-particle energy because the rate of events is to low with only 3 and 8 events in 2 minutes for bias voltages of -400 V and 400 V, respectively. The rates are even lower for lower absolute voltages.

In table 6.2 the data sets for the diamond measurements are listed. The second data set was recorded right after the pressure stability test still with the same air conditions, see section 5.2.2. For the third data set air was let into the chamber and then the chamber was evacuated again with the pump. The pump was on for five minutes and then turned off. The data set was measured right after this.

Set	Position [mm]	Charge type	Ext. amplifier	Al foil	bias voltage U [V]	ΔU [V]
1	26.39	e	yes	no	200 to 400	20
2	26.39	h	yes	no	-200 to -400	20
3	26.39	h	yes	no	-200 to -400	20

Table 6.2.: Data sets for the diamond.

6.2. Silicon diode

The analysis of the data will be discussed step by step with the data set 3.3 and 4.1, a measurement of electrons and holes respectively without external amplifier and with the unchanged α-particles. For special cases or problems other sets are used as examples.

If the external amplifier is used the program automatically detects this due to the saved settings and rescales the data point by point with the amplification factor, see section 5.1. With the other saved settings, e.g. electrons or holes, or silicon diode or diamond, the appropriate configuration values are chosen. This matters for start values or limits for fits as well as for setup values like the detector thickness and capacity.

For simplicity reasons the sign of the bias voltage is dropped. During the measurement it is important for the reverse biasing of the silicon diode or the selection of electron or hole signal for diamond measurements. For the analysis the direction of the electric field has no impact and the classification of the data is already done. So this step simplifies comparisons and also some logic of the program.

6.2.1. Averaging

Because of the stochastic nature of charge creation in matter and the trapping the measured events differ. In order to control these fluctuations 1000 events per bias voltage are recorded and then averaged. For the averaging two methods are implemented.

The first averaging method is the arithmetic mean of the voltage of each time point and the standard deviation of the mean value as uncertainty. This is the easier and more stable method.

The second method is a Gaussian fit of the voltage for each time point of the 1000 events with the mean and the standard deviation of the fit as result. In figure 6.1(a) such a fit is shown. For the fit of the first time point start parameters can be set via configuration values and for the following fits the arithmetic mean values of the previous point are used as start values. But nevertheless the fit is not always stable.

The comparison of the two methods shows that the Gaussian fit yields slightly higher mean values during the signal, see figure 6.1(b). No significant difference is observed for the noise regions before and after the signal. The noise can in general be approximated well with a Gaussian fit. The difference can be explained with the Gaussian fit weighting values which are not in the peak region less than around the mean while the arithmetic mean weights all equal. This is the strength of the fit separating signal and noise.

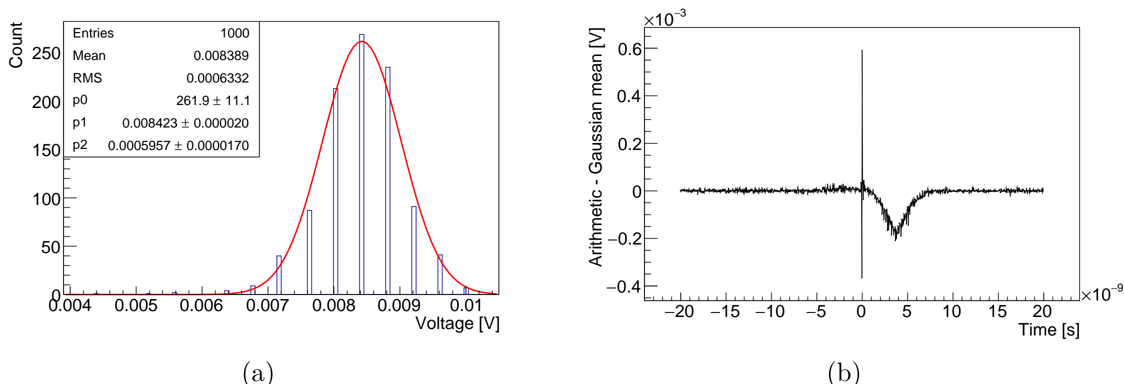

Figure 6.1.: Histogram and Gaussian fit $f(x) = p0 \cdot \exp(-\frac{(x-p1)^2}{2 \cdot p2^2})$ of a time point for bias voltage 120 V from data set 3.3 and the comparison of arithmetic mean and Gaussian fit for the whole signal in (a) and (b), respectively.

Difficulties during the averaging arise for the points around the trigger time. The trigger is always set to be at time point 0 s. As the voltage at the trigger point has to be at least as high as the trigger level the distribution is no longer symmetric for this point. The same is valid for the previous point because the value is capped below the threshold of the trigger point, which is by definition the first point over the threshold. For these points the Gaussian fit has no meaning because it is a symmetric function.

As a result of the difference in the signal region and the trigger limitation and the process stability the arithmetic mean is chosen for the averaging of the data. The Gaussian fit is still used as a control. For one test measurement the trigger level was set too low and also

noise was recorded. This showed in an even larger difference of the averaging methods in the signal region. A look at the control plots of the Gaussian fits revealed that there were two peaks in every time point histogram of that region, one from the noise and the other from the signal. The fit chose in most cases the signal peak but the arithmetic mean was lowered by the noise.

After the averaging the measurements are corrected for the offset of the noise. It is determined by a linear fit to the noise before the signal. Depending on the chosen time scale 10% to 30% of the total event time is used. The uncertainties of the fit are propagated to the uncertainty of the voltage values. This process can be nearly impossible if the pulse fills almost the whole record time because of small slopes. Except for one or two cases this was overcome by choosing an appropriate time scale when recording the data. For the exceptions the calculation could be adapted or measurements with lower bias voltage had to be excluded from the analysis. With higher bias voltages the rise times of the signal are generally shorter resulting in more time for noise before the signal.

In figure 6.2 the averaged and offset corrected measurement for all bias voltages of the data set 3.3 and 4.2 are shown in (a) and (b), respectively. The amplitude of the signal rises with the applied bias voltage for both sets. Also the signals get shorter.

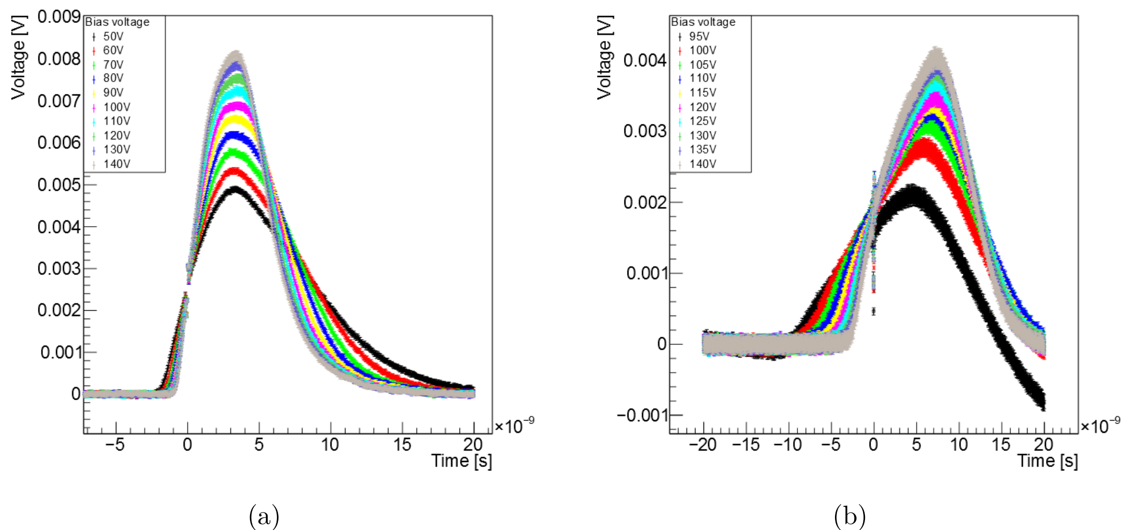

(a)

(b)

Figure 6.2.: Averaged and offset corrected data set 3.3 (electrons) and 4.1 (holes) in (a) and (b), respectively.

For the hole data set the measurement with the bias voltage of 95 V is tilted in comparison to the other measurements. This is due to the offset correction. In figure 6.3 the signal before and after the correction is shown. The noise before the signal itself has a positive slope. The correction with the linear fit to the noise results in a negative slope

for the rest of the measurement region. This measurement is still analysed on its own but excluded from combinations with the other bias voltages.

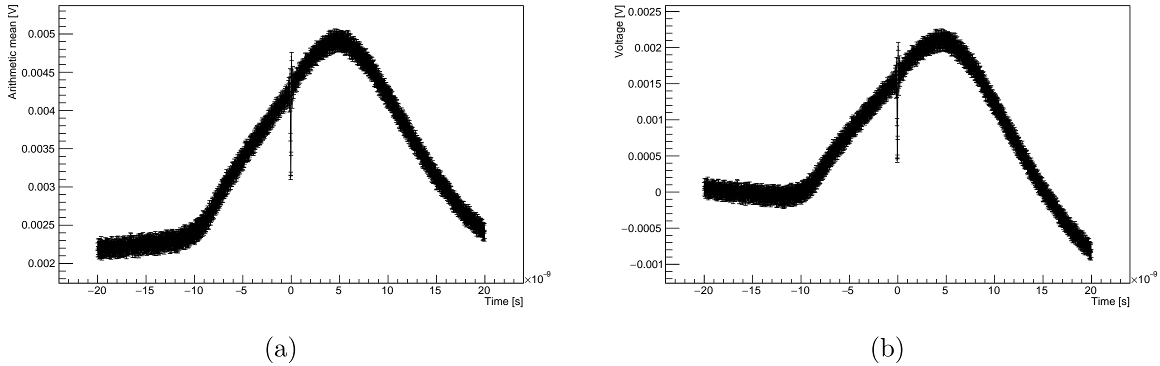

(a)

(b)

Figure 6.3.: The pulse shape before and after offset correction in (a) and (b) for the measurement with bias voltage 95 V from data set 4.1.

The comparison between the electron and the hole measurement shows many differences and one similarity. The amplitude of the signal from electrons is double the amplitude from holes in the comparable bias voltage range. For electrons the slope of the rising edge of the signal does not change a lot with rising bias voltage but the falling edge does. The signal height decreases more rapidly for higher bias voltages. The opposite is observed for holes. The falling edge stays more or less the same and the rising edge changes with bias voltage. The electron signal behaviour can be explained with an increasing drift velocity for higher bias voltages. For the holes it seems that the drift velocity is lesser than for electron.

The common feature of both data sets and all the other ones, too, is the disturbance in the rising edge at time 0 s. As mentioned before this is the trigger time. The handling of this is described in the next section.

6.2.2. Trigger ringing

In every measurement an oscillation around the trigger point is observed, see figure 6.4. In the following this is called trigger ringing. When the external amplifier is used the amplitude is smaller and in some cases barely visible as in figure 6.4(b).

A rectangular pulse from a function generator with a length of 5 ns similar to the TCT signal has been used to test the triggering of the oscilloscope and the averaging. In figure 6.5 the average of 1000 events is displayed. At the rising edge no trigger ringing is observed. This implies that the origin of the ringing is in the TCT setup and not in

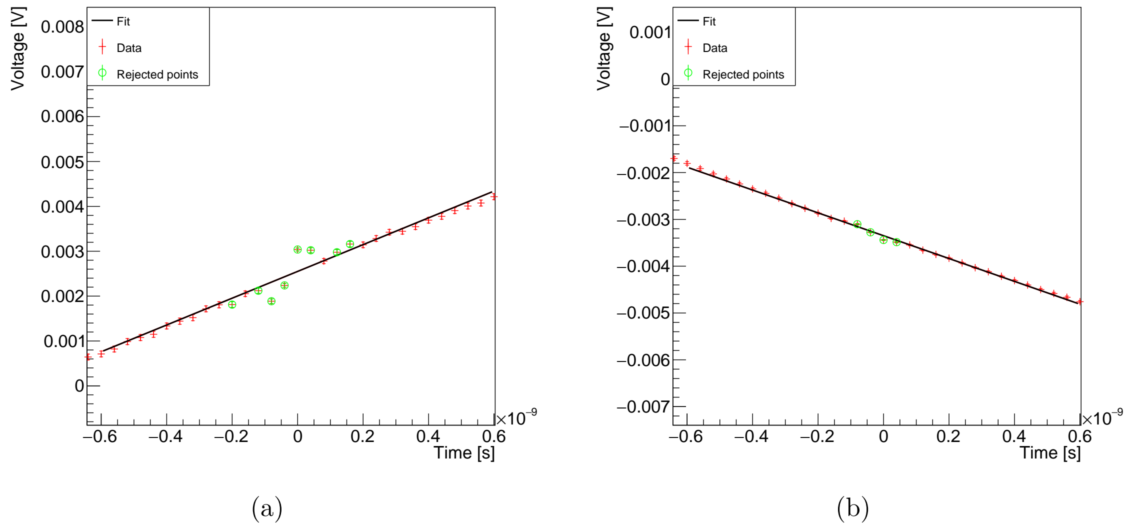

Figure 6.4.: Trigger ringing for bias voltage 120 V from data set 3.3 and 100 V from data set 3.1 in (a) and (b), respectively.

the analysis. The most likely explanation would be an impedance mismatch between the readout electronic circuit and the oscilloscope. The ringing is reduced with the external amplifier most probably because the impedances of the amplifier and the oscilloscope match. Still between circuit and external amplifier a mismatch is present resulting in the small ringing.

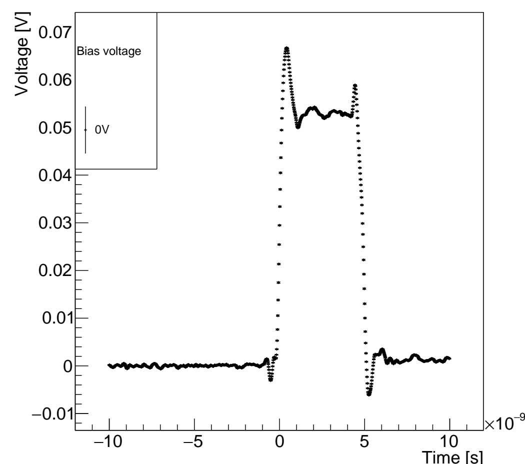

Figure 6.5.: Test measurement with function generator and oscilloscope.

The ringing has an impact on the rest of the analysis. The approach to deal with this is to exclude those points from the processing. To chose the points to omit the data

in that region is fitted with a linear function. The exact number of fit points is chosen depending on the fit points of the fit for the current described in section 6.2.3. Every data point around the trigger point which is $5\,\sigma$ off of the fit is added to the rejection list. In figure 6.4 those points are marked with a circle.

Some problems arise with the fit. The fit range has to be not to small so that the ringing disturbs the fit but also not too big so that the linear approximation is still valid. In some measurements the uncertainty of the ringing points is lower than for the other points so influencing the fit more than wanted. Problematic are also signals with a small amplitude because the trigger level has to be near the peak to avoid noise. But near the peak the slope is not linear any more, see an example in the section 6.3 for diamond results.

6.2.3. Current calculation

For the analysis the current signal is needed. So the measured voltage U has to be transformed into the current I of the drifting charge carriers. The formula for this has been calculated for the used readout electronics [18]:

$$I(t) = \frac{1}{AR_{in}} \left(R_{in} \left(C_D + C_S \right) \frac{\mathrm{d}U(t)}{\mathrm{d}t} + U(t) \right) \tag{6.1}$$

The amplification A is one in this setup as described in section 5.1.3. The input resistor R_{in} of the operational amplifier is $215\,\Omega$. In section 5.1.2 the detector capacitances C_D of the different sensors are given and the stray capacitance of the setup was measured to be $C_S = 2\,\mathrm{pF}$ [18].

The calculation of the time derivative of the voltage is done with a polynomial fit around every time point. The fit has the same number of fit points before and after the point for which the fit is done. If in the following for example the number of fit points is 10 then this has to be read as 10 before the one point and 10 after, in total 21 points. This notation is due to the processing logic. The result of such fits for the bias voltage 120 V of data set 3.3 is shown in figure 6.6 and the details of the process are explained in the following.

That the number of fit points is constant is important for the trigger ringing region. There some points are excluded from the fit. For these points additional points further away in time are used in exchange to keep the number of fit points constant. As a result the actual fit range is longer than for a fit without points to reject. The longer lever arm on the fit results in a smaller uncertainty for points with many rejected points in the vicinity.

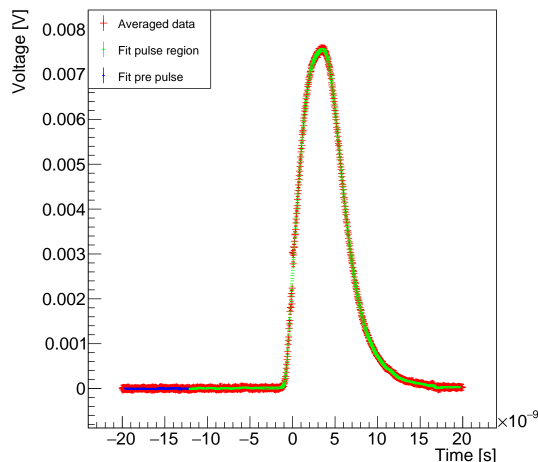

Figure 6.6.: Example of a complete fit (second order polynomial with 10 fit points) of the voltage signal for the bias voltage 120 V of the data set 3.3.

In order to determine the order of the polynomial and the number of fit points for the fit an algorithm has been implemented. It chooses from a configurable range for these parameters the best option by comparing the χ^2 values for the fits. Because the data points are correlated the χ^2_{red} for a good fit does not necessarily equal 1. Consequently, a region of the noise is fitted separately to estimate the χ^2_{red} for a good fit. This value is then used to classify the fits in the signal region.

For all data sets the second order polynomial is preferred. The number of fit points depend on the resolution of the measurement. The lowest used resolution for a measurement is 0.4 ns/point. This resolution is high enough so that higher resolutions do not reveal more structures but only add more points. This is important for the number of fit points. The same number of fit points for a higher resolution only means that more fluctuations are fitted, the result can be seen in figure 6.7. This leads to a inversely proportional scaling of the fit points to the resolution. A good factor for this is 10 points/(0.4 ns/point).

In almost all cases the choosing algorithm proposes this factor or a fit with one or two points more or less. Because the differences resulting from slightly different fit points is negligible this factor is chosen for all measurements. With this choice the data sets are consistent to each other and can be compared better.

From these fits the voltage and the derivative of the voltage for every time point is extracted and is used to calculate the current. In figure 6.8 the result for data sets 3.3 and 4.1 is displayed. The amplitude of the current for electrons is a bit more than double the one for holes. The rising edge for electrons and the falling edge for holes are more or less independent of the bias voltage. A dependence from the bias voltage is observed for

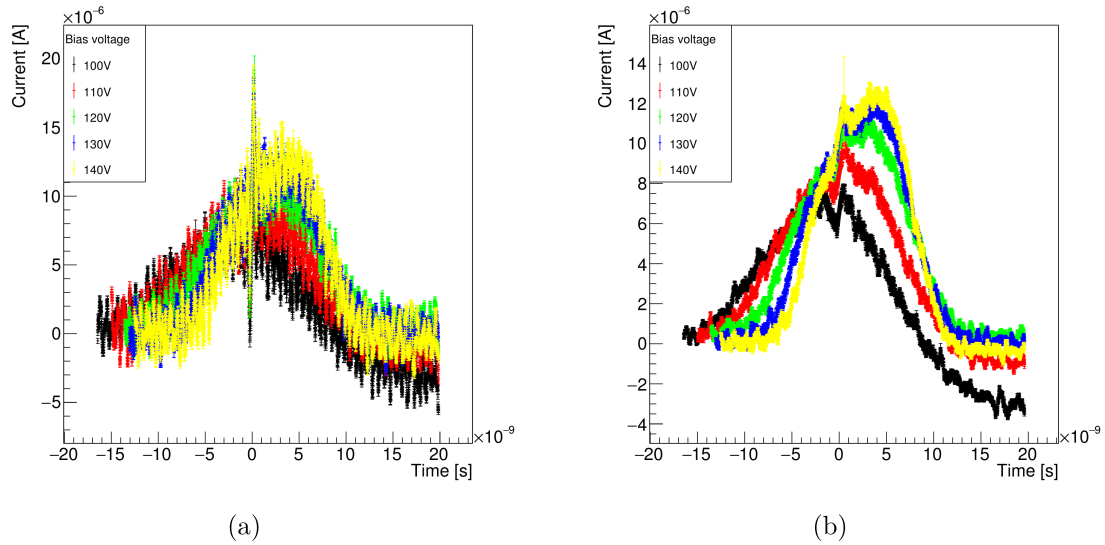

(a)

(b)

Figure 6.7.: Current of the same data set with 20 fit points and 50 fit points for the voltage fit in (a) and (b), respectively.

the other edges.

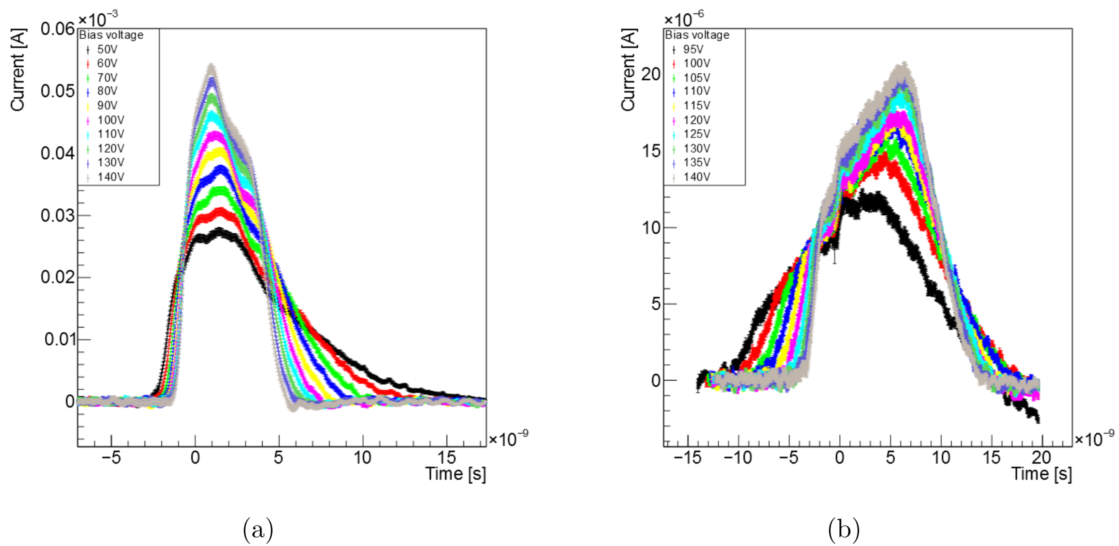

(a)

(b)

Figure 6.8.: Calculated current for the data sets 3.3 and 4.1 in (a) and (b), respectively.

For bias voltages larger than 60 V the falling edge for electrons is a clear edge and not only an exponential decay as for lower bias voltages. This implies that with this bias voltage and higher the electrons reach the electrode as one package. The non zero width of the edge can be explained by a diffuse package. With its arrival almost no electron is left to drift and result in a current. For lower bias voltages the electrons arrive not at

one moment but distributed over a longer time. The depletion voltage for this diode is measured as 56.2 V [18]. For bias voltage smaller than this the spread of the charge cloud is expected to be even larger because of zones in the material where diffusion dominates the movement. This can be observed in the broad falling edges for electron signal for bias voltages lower than the depletion voltage. Due to this measurements with bias voltages lower than 60 V are excluded from analysis which combine results from different bias voltages.

Before the falling edge the signal from electrons decays exponentially. For holes the signal rises first with an edge and then slower until the falling edge. This behaviour has been observed before, see section 4.3, and has been appointed to a positive space charge in the sensor.

After the trigger time still a disturbance can be observed for both electron and hole signals. For data set 4.1 this is a step in the current. Other hole data sets exhibit a shallow peak on top of the current at the same position, see figure A.15(b). For electrons it is a small decrease and then increase of the current. It is not so clear for electrons because with higher bias voltages the feature is swallowed by the high slope of the rising edge. But still two different decays are observed for high bias voltages. The origin of this behaviour can be seen in figure 6.9 where the measured voltage and the fitted voltage is displayed in the region of the rising edge for the bias voltage 110 V of the data set 4.3. At the trigger the measured voltage has a step and the slope gets steeper after. This feature is on a larger time scale than the trigger ringing so this could be a extension of the same problem or an other one. The appearance at the same time point hints strongly at a correlation. Also such behaviour is not observed for the function generator test.

For the further analysis, however, the impact of this seems relatively small as long as the additional peak for holes is not higher than the current amplitude. For the analysis the length of the signal is needed, which is not altered and the integral of the signal, which is changed by the additional height. But in comparison to the whole signal this addition is negligible as it is only short in time.

6.2.4. Drift velocity and charge

The calculation of the drift velocity and the charge breaks down to determine the start and the end of a signal. Three different approaches have been tried ramping up in difficulty and are here described to explain why the simplest one is chosen in the end. The description is based on the idea of a positive signal to avoid confusion but for negative currents only the comparisons have to be adapted to the extra sign.

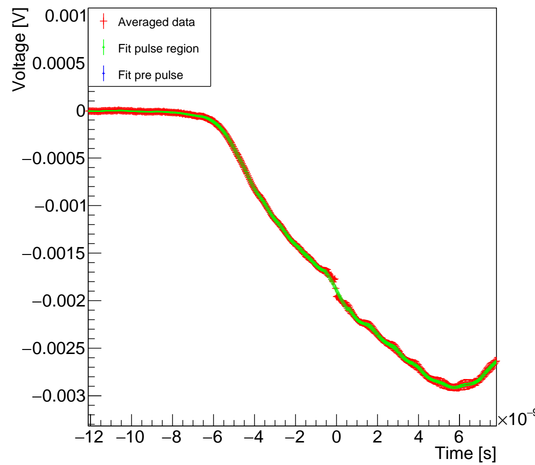

Figure 6.9.: Measured and fitted voltage with a bias voltage 110 V for data set 4.3 zoomed in at the rising edge.

Start and end time of a signal

The simplest method is comparison with a threshold. When the current is higher than the first threshold this is the start time of the signal. When the current drops below a second threshold the signal ends there. The only question with this is what thresholds can be chosen reliably for an automation. But this problem is the same for all methods so it will be discussed after the methods.

The second, more advanced, method is a fit to the edges of the signal with an error function. This approximates the shape of the edges well. But the fit range has to be set for the fits. So the first method is used to set start and end for each fit.

The shape of the signal is not a rectangular pulse. As seen before the pulse decreases for electrons in between the edges and rises for holes. This extra slope should not be included in the fit range of the error function fit because it is not part of the edge. So the change in the slope from middle part to edge or the other way around has to be detected. The implementation was attempted by calculating the derivative of the current. It is calculated in a similar way to the derivative of the voltage. In the derivative local minima and maxima are searched to find these changes. But there are many fluctuations which create local minima and maxima so the algorithm gets stuck on these. In the end it was not possible to automate this search in a reliable way for different measurements.

Without an automatic fit range the option remaining is the threshold method. For the rising edge the threshold is chosen as 10% of the maximum current of each measurement. Due to the different falling edges for electrons and holes the threshold is dependent on the type of signal. 50% of the maximum current is chosen for holes because then most of the

charges arrive. For electron signals the falling edge is divided into the exponetial decay and the arriving edge. Therefore a lower threshold of 25% is chosen. In the following condition is used as a synonym for the threshold level in units of the maximum current, meaning condition equal 1 is the maximum current.

In order to optimize the threshold value for each measurement the edges are mapped with different threshold values. Then the times of the thresholds are plotted against their condition and fitted with a linear fit to get the time of the desired threshold. The different shapes of the edges for electrons and holes are taken into account for the mapping. In figure 6.10 these plots are displayed.

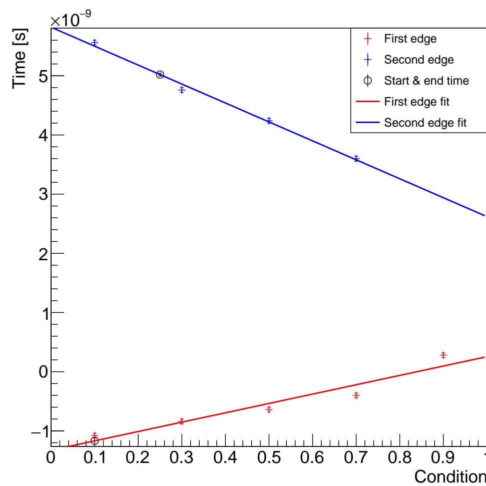

Figure 6.10.: Determination of the start and end time of the signal from data set 3.3 with bias voltage 120 V.

In order to compare the different bias voltages of one data set better the current is also displayed with the start time of each signal set to the origin of the time axis. These plots are called shifted current to differentiate them from the other current plots. With this shift the length of the signals can be compared easier.

Transit time and drift velocity

The transit time t_t of the charges is calculated as the difference of pulse end time t_e to pulse start time t_s. With the sensor thickness D the drift velocity is calculated: $v_D = D/t_t$. The uncertainties of the thickness and the transit time are propagated to the velocity.

Charge

The charge of the signal is calculated as the integral of the current from the start time to the end time. For this a *root* function exists which unfortunately does not yield the uncertainty of the integral. So dedicated algorithm is used. It takes the current values and their uncertainty to randomly generate new current distributions. The current at one point is used as the mean of a Gaussian distribution and the uncertainty as the standard deviation. From this distribution a new current value and uncertainty is randomly generated for this point. This is done for every point individually and with this new current the integral is calculated again. The resulting charge is put in a histogram and the process is repeated in total 1000 times. The histogram is then fitted with a Gaussian, see figure 6.11. Due to the construction the mean value of the Gauss is the same as the values provided by the *root* function. The standard deviation of the fit is taken as the uncertainty of the charge.

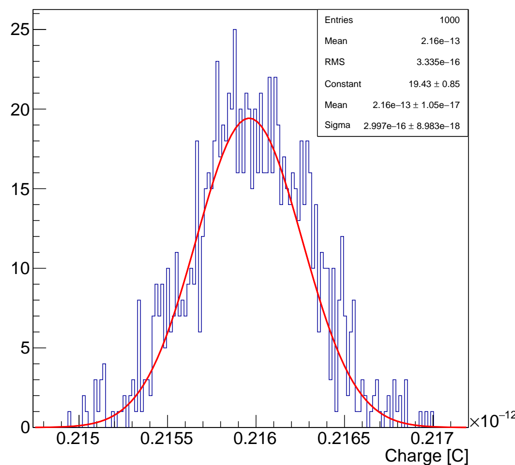

Figure 6.11.: Histogram for the calculation of the uncertainty of the charge for bias voltage 120 V of data set 3.3.

Influence of different thresholds

The influence of different thresholds on the drift velocity and the charge are investigated. In figure 6.12 the relative difference of the drift velocity and the charge with the normal threshold to the test thresholds are displayed. In general the influence on the drift velocity is higher than on the charge. This can be easily explained with the transit time in the denominator for the calculation of the drift velocity. The charge does not change as much, because the fast rise of the edges results in a small area to integrate in that region.

For small changes of the threshold conditions of 10% per edge a systematic uncertainty of roughly 8% to 15% is estimated for the drift velocity and 3% to 9% for the charge depending on the data set and the applied bias voltage. This uncertainty is not added to the uncertainty of the values because the influence of the measurement and not of the analysis is at this stage of understanding of the setup of more importance. Tests however showed, that the derived values from the drift velocity and charge with the added systematic uncertainty do not change significantly. Only the uncertainty of the values rises, as it is expected.

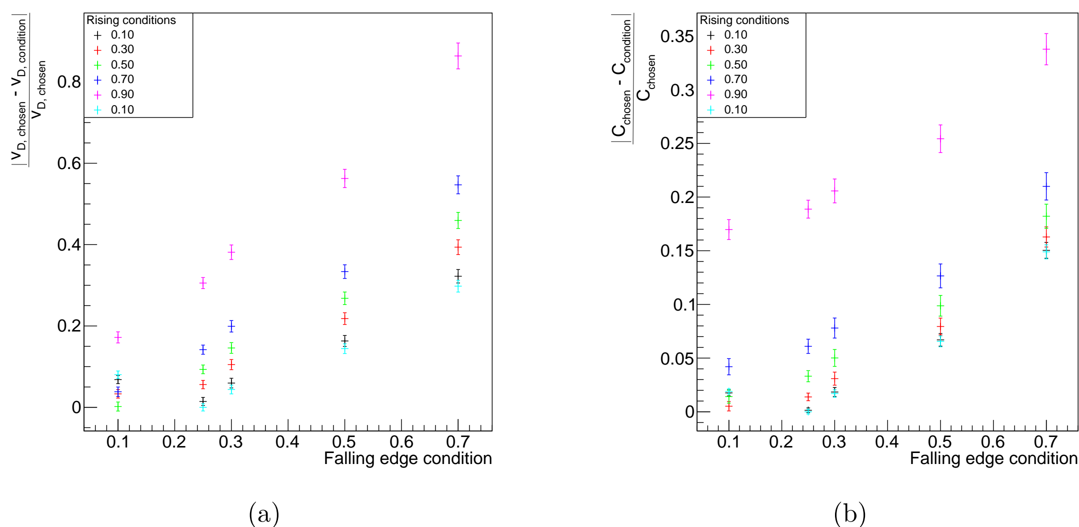

Figure 6.12.: Relative difference of the drift velocity and the charge with respect to different start and end thresholds for the bias voltage 120 V of the data set 3.3.

6.2.5. Mobility

As discussed in section 4.4 the mobility of the charge carriers is connected to the drift velocity and the electric field. The electric field is approximated constant $E = U/D$. In figure 6.13 the drift velocities of the data sets 3.3 and 4.1 are plotted against their corresponding electric field.

The equation (4.5) is used to fit the drift velocities for each data set. Excluded are measurements with bias voltages equal and below 60 V for the reasons discussed already. For this fit the saturation velocity v_{sat} is limited to the values at room temperature for electrons 105 µm/ns and for holes to 81 µm/ns [21]. The resulting mobility is $\mu_e^0 = (1329 \pm 4)\,\mathrm{cm^2/Vs}$ and $\mu_h^0 = (408.2 \pm 0.2)\,\mathrm{cm^2/Vs}$ for electrons and holes, respectively. The

saturation velocities are at their limit. If the limits are set higher the mobility changes only little and the velocity is at the new limit. Especially for hole measurements the shape of the fit does not change much with this parameter. In general the fits for hole data is not so good as can be seen in figure 6.13. This implies that the model is not good for lower drift velocities.

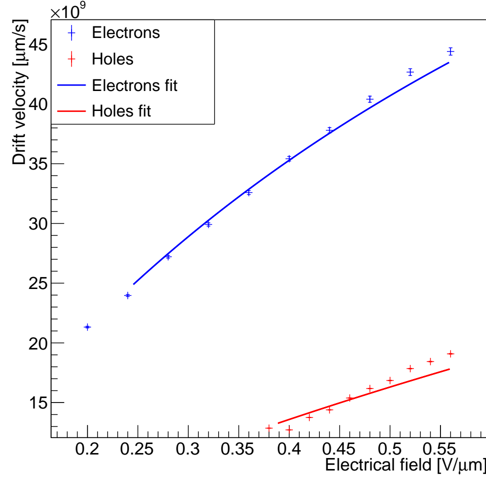

Figure 6.13.: Drift velocity of the data sets 3.3 (electrons) and 4.1 (holes) displayed against the electric field with a fit for each according to equation (4.5).

The literature values for the mobility are $\mu_e^0 = 1450\,\mathrm{cm}^2/\mathrm{Vs}$ and $\mu_h^0 = 440\,\mathrm{cm}^2/\mathrm{Vs}$ [22]. The results from these two data sets are in the same order of magnitude as the literature values. The low uncertainties are surprising because the fits seem not that good.

In section 6.2.8 the results for the other data sets are presented. In that context the result presented here will also be discussed.

6.2.6. Trapping lifetime

With the charge and the transit time of a signal for different bias voltages the total deposited amount of charge Q_0 and the lifetime of the charges before they are trapped τ can be estimated. For this the values of the charge and transit time are plotted for one data set and then fitted with the following formula which derives from equation (4.6):

$$Q = Q_0 - \frac{t_t}{2\tau} Q_0 \tag{6.2}$$

In figure 6.14 this is done for the data sets 3.3 and 4.1. The resulting lifetimes are $\tau_e = (60 \pm 0.3)\,\mathrm{ns}$ and $\tau_h = (60 \pm 0.04)\,\mathrm{ns}$. For the total charge the values are $Q_0^e = (228.3 \pm 0.1)\,\mathrm{fC}$ and $Q_0^h = (223.01 \pm 0.08)\,\mathrm{fC}$. The uncertainties of the values are

very small though the fit is not that good. This implies that the measurements are dominated by systematic uncertainties. Since the values for the lifetime are so similar it was tried to vary the fit with the start values to test whether the fit got stuck somewhere. But the result was the same.

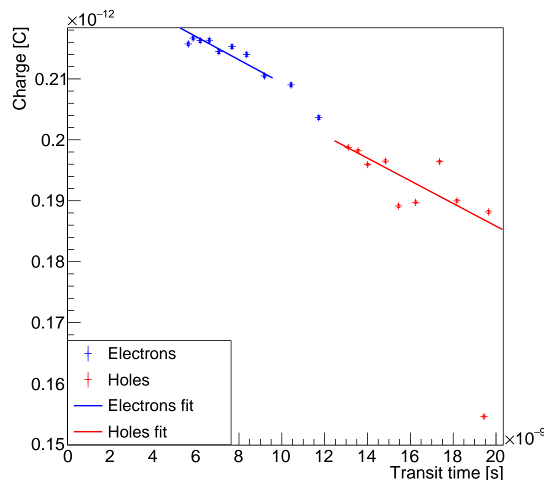

Figure 6.14.: Charge as a function of transit time for the data sets 3.3 (electrons) and 4.1 (holes) with a fit each to equation (6.2).

With the total charge and the energy of the α-particles the energy E_{eh} needed to create an electron-hole pair is calculated for electrons to $E^e_{eh} = (3.915 \pm 0.002)\,\text{eV/pair}$ and for holes to $E^h_{eh} = (3.885 \pm 0.001)\,\text{eV/pair}$. These values are near the literature value of $3.6\,\text{eV/pair}$.

In comparison to the other data sets the results are discussed in section 6.2.8.

6.2.7. CCD

The charge collection distance CCD can be calculated using two different methods, which will be introduced briefly.

Approximation

If the CCD is significantly smaller than the sensor thickness then the CCD is approximated with the following formula:

$$\text{CCD} = \frac{Q}{Q_{exp}} D \qquad \text{for CCD} << D \tag{6.3}$$

The expected charge Q_{exp} can be calculated with the energy of the α-particle and the literature value for the needed energy per electron-hole pair, see table 3.1. For the data sets 3.3 and 4.1 the result of this calculation is displayed in figure 6.15 for the different bias voltages used.

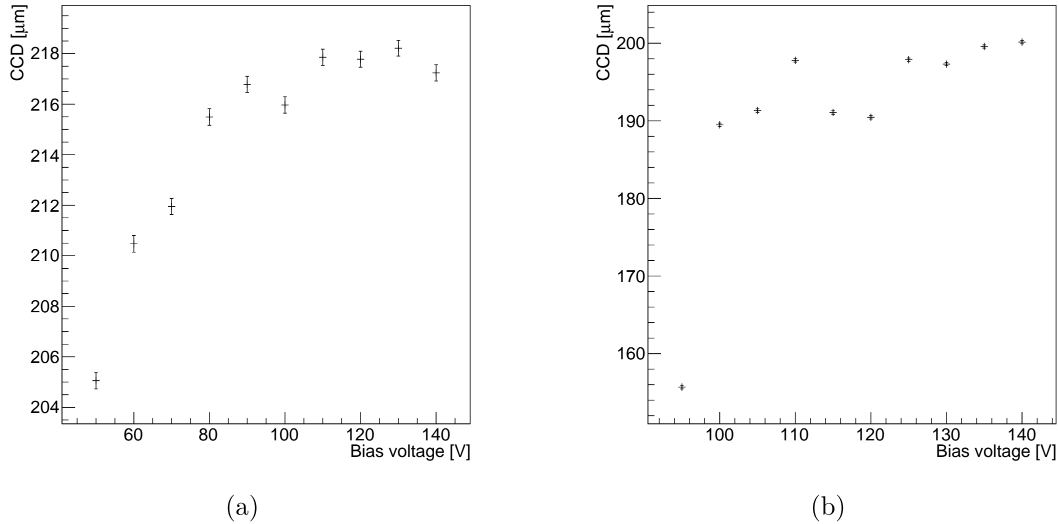

Figure 6.15.: Approximation of the CCD with the equation (6.3) for data sets 3.3 and 4.1 in (a) and (b), respectively.

For both data sets the CCD is lower than expected with values of 200 µm lower than expected as uniradiated silicon has very few traps. But since the CCD should exceed the sensor thickness this approximation is not valid. The reason to show it here is that the method is used later for the diamond data and to prove that a better one has to be used for silicon.

Combination of mobility and lifetime

The reliable option to calculate the CCD is given in equation (4.7). But it requires the mobility and the lifetime for electrons and holes which has been calculated before. For data set 3.3 and 4.1 the CCD is calculated to:

$$\mathrm{CCD} = (10422 \pm 54)\,\mu\mathrm{m}^2/\mathrm{V} \cdot E.$$

With the approximation of a constant electric field $E = U/D$ in the sensor this can be written as:

$$\text{CCD} = (41.7 \pm 0.8)\,\mu\text{m/V} \cdot U.$$

This result leads to a higher CCD than the sensor thickness for every used bias voltage, which is as expected.

6.2.8. Results and comparisons between data sets

In appendix A the plots for all silicon data sets are displayed. In general the signals with the same settings of the setup have the same height and length. The length of the signal depends on the selection of electron or hole signal only. With the lower energetic α-particles the amplitude of the signal is for electrons roughly 20 µA and for holes 8 µA smaller, which equals to 36% and 40%, respectively. This shows that the energy of the α-particles influences electron and hole signal equally as expected, because they are created as pairs.

The current for measurements with the external amplifier exhibit an undershoot after the signal. This could indicate that with the amplifier the capacitance of the setup is changed. But this has not been further investigated. An additional observation with the amplifier is that it changes the sign of the measured voltage.

Most of the measurements of hole signal suffer from the disturbance at the trigger point. For electrons this is not so obvious, as the rising edge is at that point already very steep.

The results of the analysis for all silicon data is summarized in table 6.3.

The uncertainties are very small although some fits are not that good and have to be treated carefully. The results depend strongly on the start and the end of the signal. The influence of the signal and its uncertainty is minor. Accordingly even data sets with large disturbances at the trigger, e.g. 5.2, provide results not too different to the other data sets. The influence of the measurement uncertainty is small as long as the edges of the signal can be reliably identified. Systematic uncertainties from the analysis could have a bigger impact. A first attempt to investigate the influence of different thresholds on the drift velocity and charge has been shown. These could not be included due to too little time to test it properly.

The results for the mobility are in the right order of magnitude compared to the literature values of $\mu_e^0 = 1450\,\text{cm}^2/\text{Vs}$ and $\mu_h^0 = 440\,\text{cm}^2/\text{Vs}$ for electrons and holes, respectively [22]. The spread of the different measurements is much large than the uncertainties of the single measurements support. This indicates again that systematic uncertainties

Set	μ_0 [cm^2/Vs]	τ [ns]	Q_0 [fC]	E_{eh} [eV/pair]
electrons				
1.1	1334 ± 2	60 ± 1	227.3 ± 0.1	3.932 ± 0.002
1.2	1500 ± 11	31 ± 1	150.9 ± 0.8	4.30 ± 0.02
2.1	1355 ± 2	44 ± 2	231.6 ± 0.8	3.86 ± 0.02
2.2	1584 ± 5	18.0 ± 0.3	233.5 ± 0.9	3.83 ± 0.02
2.3	1730 ± 30	14.1 ± 0.2	157.2 ± 0.7	4.13 ± 0.02
3.1	1591 ± 5	17.7 ± 0.3	233.8 ± 0.8	3.82 ± 0.01
3.2	1800 ± 30	13.3 ± 0.2	156.2 ± 0.7	4.15 ± 0.02
3.3	1329 ± 4	60.0 ± 0.3	228.3 ± 0.1	3.915 ± 0.002
3.4	1400 ± 20	49 ± 3	145.7 ± 0.7	4.45 ± 0.02
holes				
4.1	408.2 ± 0.2	60.00 ± 0.04	223.01 ± 0.08	3.885 ± 0.001
4.2	373.2 ± 0.2	33.0 ± 0.5	158.4 ± 0.8	4.10 ± 0.02
4.3	459.2 ± 0.4	22.8 ± 0.1	236.2 ± 0.6	3.95 ± 0.01
4.4	536.3 ± 0.3	14.40 ± 0.08	160.1 ± 0.8	4.05 ± 0.02
5.1	462.2 ± 0.3	21.00 ± 0.09	241.6 ± 0.6	3.699 ± 0.009
5.2	492.8 ± 0.3	24.5 ± 0.2	130.4 ± 0.5	4.98 ± 0.02
5.3	362.9 ± 0.2	60.00 ± 0.01	232.0 ± 0.1	3.852 ± 0.002
5.4	361.0 ± 0.1	60.00 ± 0.01	143.41 ± 0.07	4.525 ± 0.002

Table 6.3.: Results for the silicon diode.

dominate the results.

The lifetime before trapping is also wide spread from 13 ns to 60 ns. Within this range no difference between electron and hole signal is observed.

In contrast to the lifetime the original deposited charge is more confined. The maximum difference between two measurements is roughly 20 fC for both the normal α-particle energy and the attenuated, which equal to 8% and 12%, respectively. The resulting energy needed to create one electron-hole pair is systematically higher than the literature value of 3.6 eV/pair. This indicates that some energy is already lost in the residual air in the vacuum chamber and the SiO_2 passivation layer of the diode. At least 15 fC are missing for the lowest measured value of 3.8 eV/pair in comparison to the literature value.

The same measurements have been done for different positions of the silicon diode to the source. Without going into the detail of every comparison it can be said that there is no dependence of the results with respect to the position. The differences between the measurements with same settings except the distance is smaller than the difference between measurements at the same position with other settings changed.

The only result that depends on the type of charges is the mobility. As expected it is higher for electrons than holes. The total charge is independent of the charge carrier

type. Everything but would be surprising due to the creation of the charges as pairs.

Comparing data sets with the same settings except the energy of the α-particles shows a systematic higher energy needed to create an electron-hole pair for the measurements with attenuated energy. This could mean that the thickness of the Al foil is not correct and consequently the reduction of the energy is not calculated correct either.

When the external amplifier is used the mobility for electrons and holes is higher than without the amplifier. Also the lifetime is then lower.

CCD

With the mobility and lifetime for electrons and holes the CCD is calculated for data sets 3.x and 4.x, as the distance to the α-source is nearly the same for them. The data sets with the same settings are combined. In table 6.4 the results are displayed.

Set e	Set h	CCD/U [µm]
3.1	4.3	15.5 ± 0.4
3.2	4.4	12.7 ± 0.4
3.3	4.1	42 ± 1
3.4	4.2	32 ± 2

Table 6.4.: Calculated CCD with the mobility and lifetime for electrons and holes.

For the measurements without amplifier the CCD/U is more than double the one for the measurements with amplifier. One reason for this could be that the values for the capacitances in the current calculation have to be adapted for the measurements with amplifier as mentioned before. As seen in the previous comparison the mobility and the lifetime values of measurements with and without external amplifier differ. Another problem is the disturbance at the trigger point. For data set 4.4 it is higher than the actual amplitude of the current. With such underlying problems it is not easy to explain exactly such differences but a connection to the amplifier is possible.

However the order of magnitude of the result seems to be correct because signal of electrons can be observed for bias voltages higher than 10 V. Also with the previous setup [18] the result for the silicon diode was CCD/$U = (23 \pm 3)$ µm which lies in between the derived values here.

6.3. Diamond

6.3.1. TCT voltage and current

In figure 6.16 the TCT voltage signal from the diamond for electrons and holes is displayed. The signal amplitude is 1.4 mV and only possible to measure if the external amplifier is used. Also the signal very short. No difference for electron and hole signal is observed except the sign of the voltage which is due to the different charge carriers.

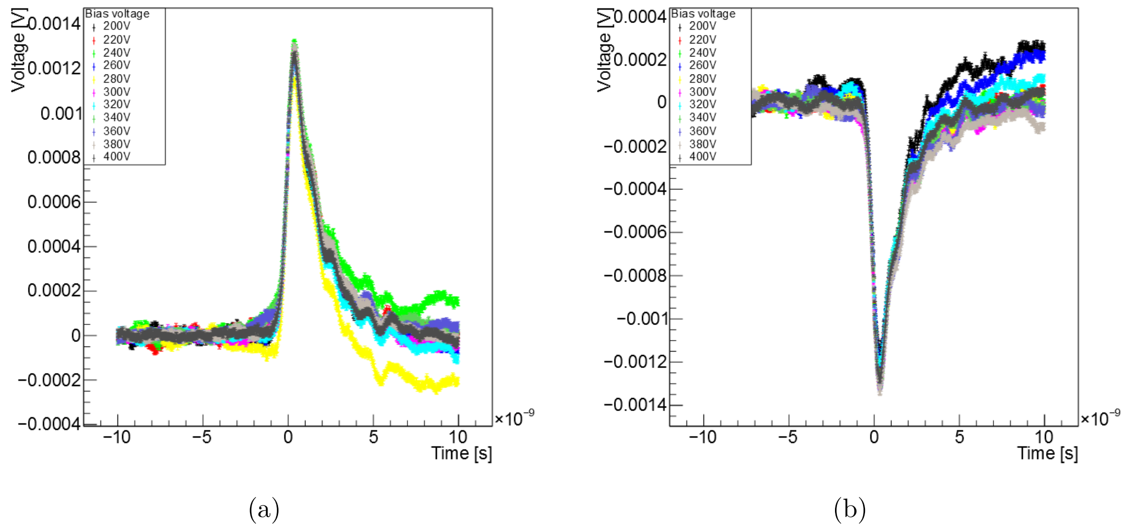

Figure 6.16.: Measured voltage signal for data set 1 (electrons) and 3 (holes) in (a) and (b), respectively.

After the signal the measured voltage differs for the different bias voltages in one data set. This is due to a difficult offset correction, as the noise before the signal is not flat but has non zero slopes for short times. These slopes can tilt the correction slightly.

The falling edge is not smooth but has several changes of the slope. At one point the slope is almost zero. Such a behaviour is not observed for the silicon diode. There, only one clear edge marks the arrival of the charge carriers.

The derived current is shown in figure 6.17 and in figure 6.18 the signal region is displayed. No significant differences are seen for the different bias voltages in the data sets. The signals are very short with only 1 ns to 1.5 ns compared to the silicon signal. The amplitude for electrons and holes is the same with roughly 14.5 µA. The peak of the signal has a different slope for different bias voltages. This is an artefact of the correction of the trigger ringing because the trigger level is near the peak voltage. A lower trigger level is not possible due to the amplitude of the noise.

After the signal the current oscillates for roughly 5 ns with decreasing amplitude. This behaviour is not observed for the silicon diode. Its origin could be the changes of the slope in the falling edge of the measured voltage.

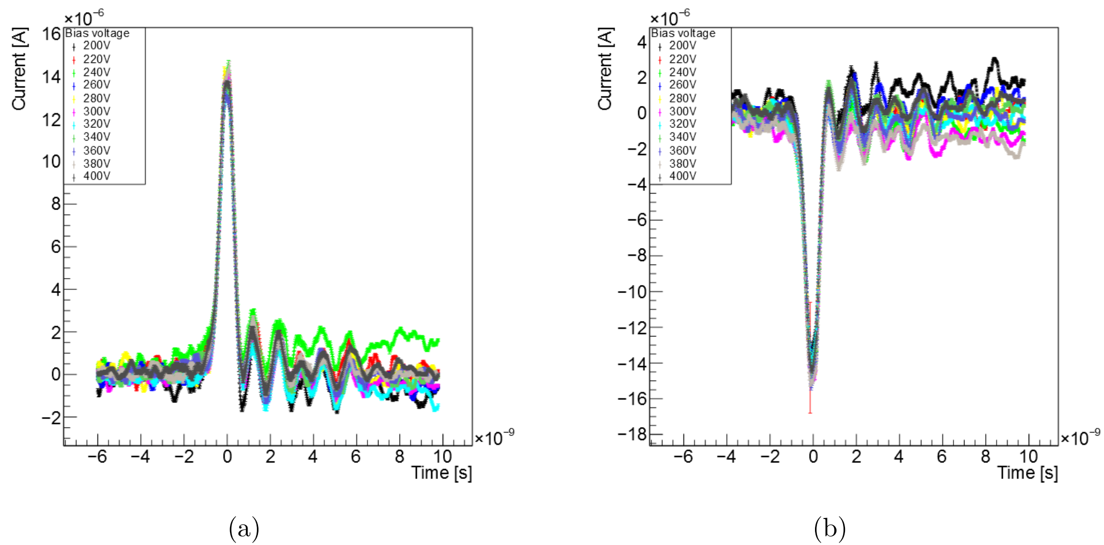

Figure 6.17.: Current for the diamond data set 1 (electrons) and 3 (holes) in (a) and (b), respectively.

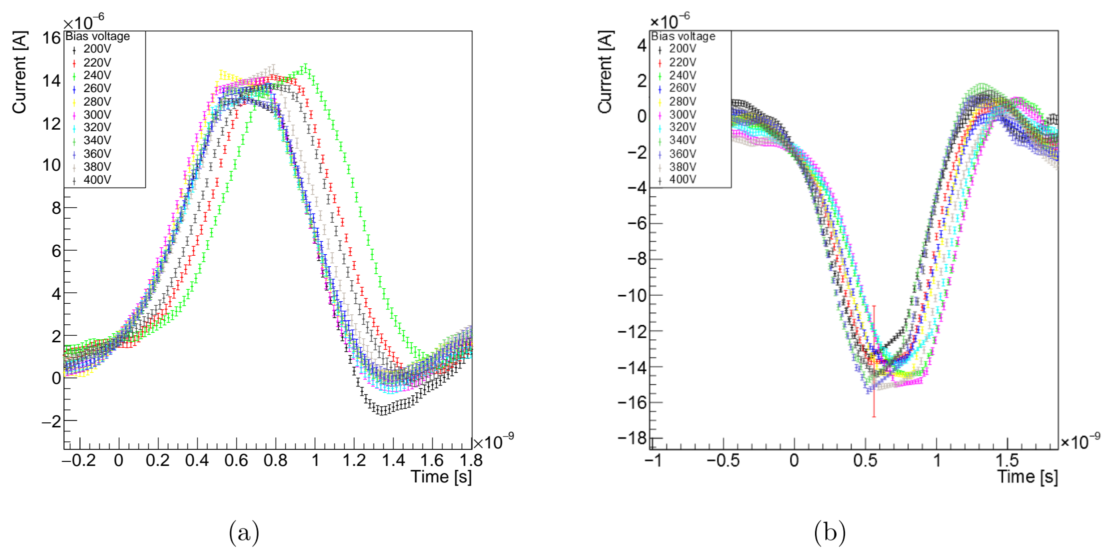

Figure 6.18.: Current with shifted start point to 0 s, signal region of data set 1 and 3 in (a) and (b), respectively.

Since there is no significant difference between the measurements with different bias voltages the methods to derive the mobility and the lifetime of the charge carriers can

not be used. In the appendix A.2 the failed attempts can be found. It shows that the drift velocity is saturated for all used bias voltages. The transit time is around 1 ns with a spread of 0.1 ns. A estimation of the lifetime is done with equation 6.2 with the mean charge of all measurements of (9.8 ± 0.5) fC and the literature value of the total charge: $\tau = (0.58 \pm 0.06)$ ns. This is half of the transit time and implies a huge amount of traps. As the sample is an old one which has been irradiated before this result is not unexpected. It also explains the large bias voltages needed to observe the signal because high drift velocities are needed to compensate the trapping.

6.3.2. CCD

The approximate calculation of the CCD is possible because it only needs the charge of the signal. In figure 6.19 the results for data sets 1 and 3 are displayed. For electron and hole signal the CCD is in the range of 50 µm to 60 µm. The mean value for electron and holes calculates to:

$$\overline{\text{CCD}}_e = (56 \pm 3)\,\mu\text{m},$$
$$\overline{\text{CCD}}_h = (58 \pm 4)\,\mu\text{m}.$$

The total mean of all three measurement is then:

$$\overline{\text{CCD}} = (57 \pm 2)\,\mu\text{m}.$$

For the same diamond and with the TCT setup before the changes discussed in this thesis the CCD has been determined to be in the range of 35 µm to 50 µm [18]. The small difference to the result can be easily explained with small differences in the analysis especially considering the short signal times.

Keeping in mind the observed lower deposition of charges in silicon of at least 15 fC the CCD of the diamond could be higher, too, if the charges are lost in the residual air in the chamber and not silicon specific. A calculation of the correction is not possible because the measured charge for the diamond is only the charge with losses to trapping. For the correction the total deposited charge would be needed.

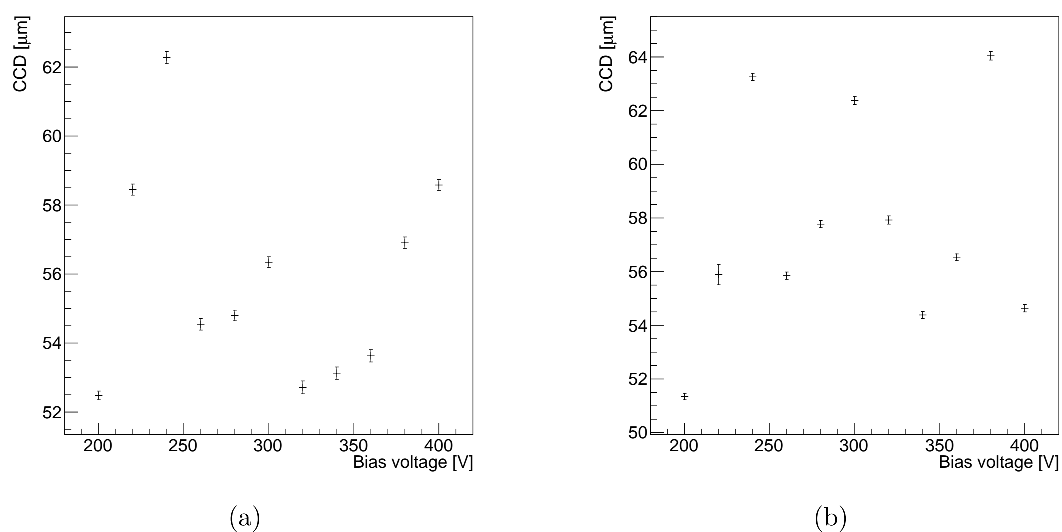

(a)

(b)

Figure 6.19.: CCD calculated for the diamond data sets 1 and 3 in (a) and (b), respectively.

7. Summary and outlook

For high energy experiments particle detectors are needed which have to be more and more radiation tolerant as the experiments are upgraded. A radiation tolerant material is diamond, especially synthesised scCVD and pCVD diamond. To test its capabilities as a detector material the transient current technique (TCT) is used. With it the behaviour and properties of charge carriers in matter can be investigated. One key quantity is the charge collection distance CCD which describes how well charges can travel in the material.

TCT signals have been measured for a silicon diode and a pCVD diamond with an α-source. To be able to do this, changes to a previous setup have been made. Now one readout electronic can be used for different samples instead of special readouts for each sample. This allows easier handling and reduces the systematic differences between different samples. With the changes, the setup also seems more stable than before.

The silicon diode has been used to evaluate different settings of the setup. The results are in the order of the literature values but vary for different settings. The most stable result over the different measurements is the estimation of the deposited charge and from that the energy needed to create a electron hole pair in silicon with 3.8 eV/pair to 4.5 eV/pair. This is systematically higher than the literature value which suggests that not the whole energy of the α-particles is deposited in the silicon but also some is lost before. The uncertainties of the results derived from the measurement uncertainties are very low and do not support the spread of the results. This implies that the systematic uncertainties dominate the measurements.

Even the small signals from the diamond with an amplitude of 1.4 mV could be measured with the setup. The CCD of the diamond could be calculated to (57 ± 2) µm which is in good agreement to previous measurements for the sample.

One big problem with the measurements was a disturbance at the trigger point of the oscilloscope. It is most probably due to an impedance mismatch between the readout electronics and the oscilloscope. For the time being it is tried to correct it in the analysis of the data but a improvement of the setup would be the step to go for reliable measurements.

In the analysis of the measurements the main focus was set on propagating all measure-

ment uncertainties to the resulting values. Different settings for the analysis have been tried and optimized. Their impact on the results could not be quantified in systematic uncertainties. This would be an other improvement of the results.

The analysis itself could be further improved and extended, e.g it should be possible to extract the capacitance in the setup from the recorded signal.

All in all it has been shown that it is possible to measure TCT signals from silicon and diamond with the setup. In a next step it would be interesting to study more diamonds to classify its capabilities as particle detector.

A. Data and Results

A.1. Silicon diode

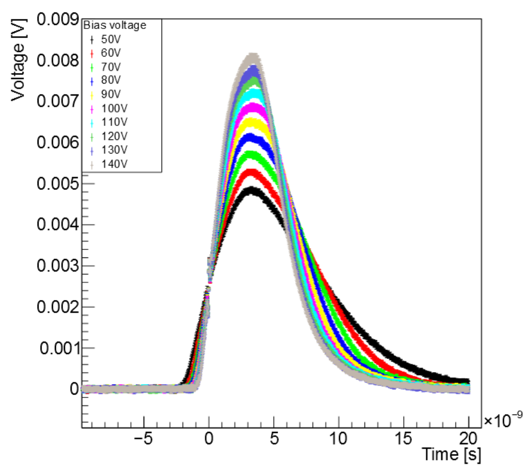

(a) TCT voltage signal.

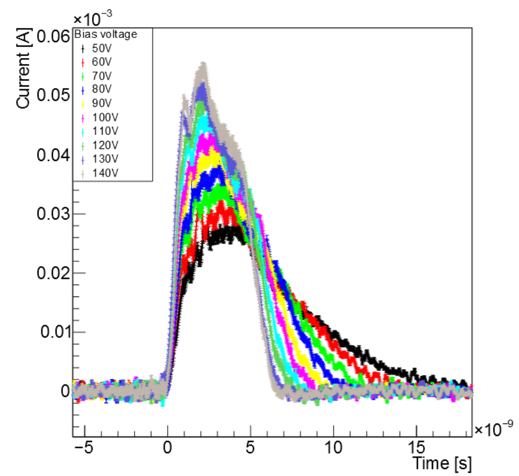

(b) Shifted current.

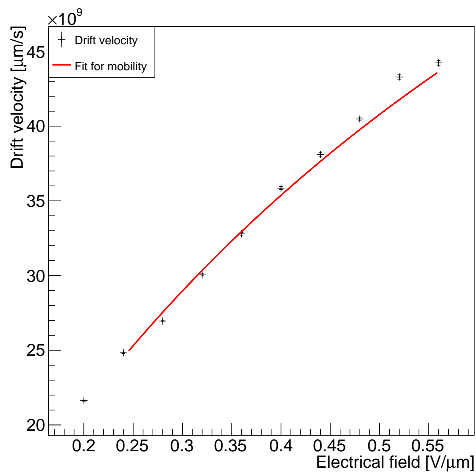

(c) Mobility fit.

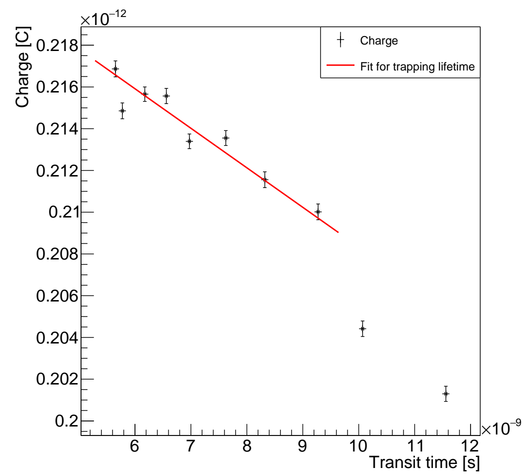

(d) Lifetime fit.

Figure A.1.: Data set 1.1.

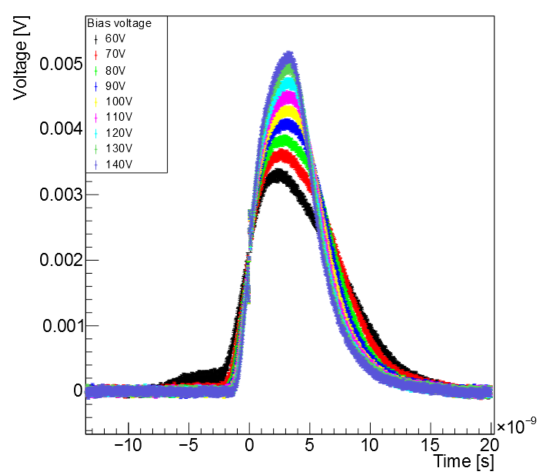

(a) TCT voltage signal.

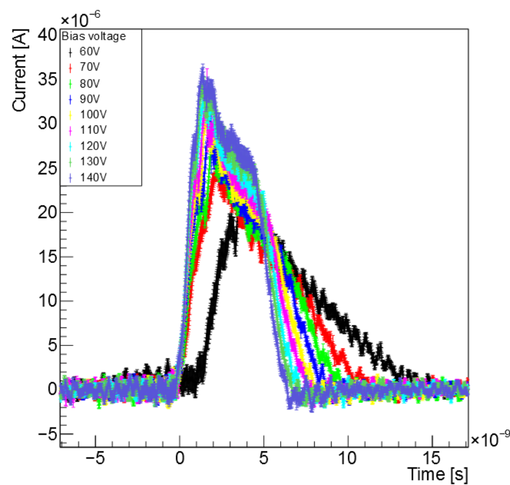

(b) Shifted current.

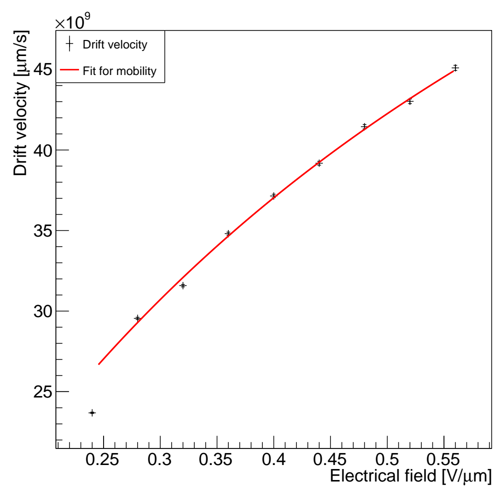

(c) Mobility fit.

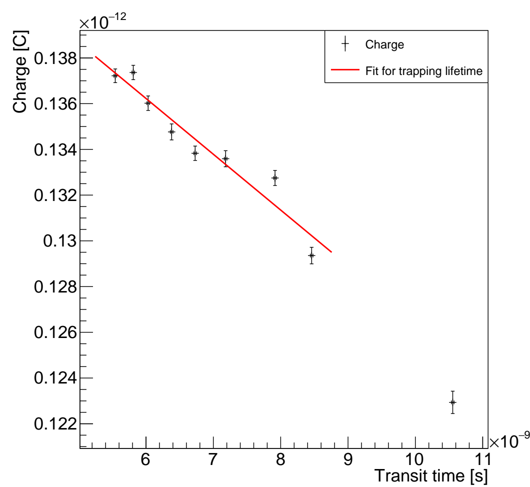

(d) Lifetime fit.

Figure A.2.: Data set 1.2.

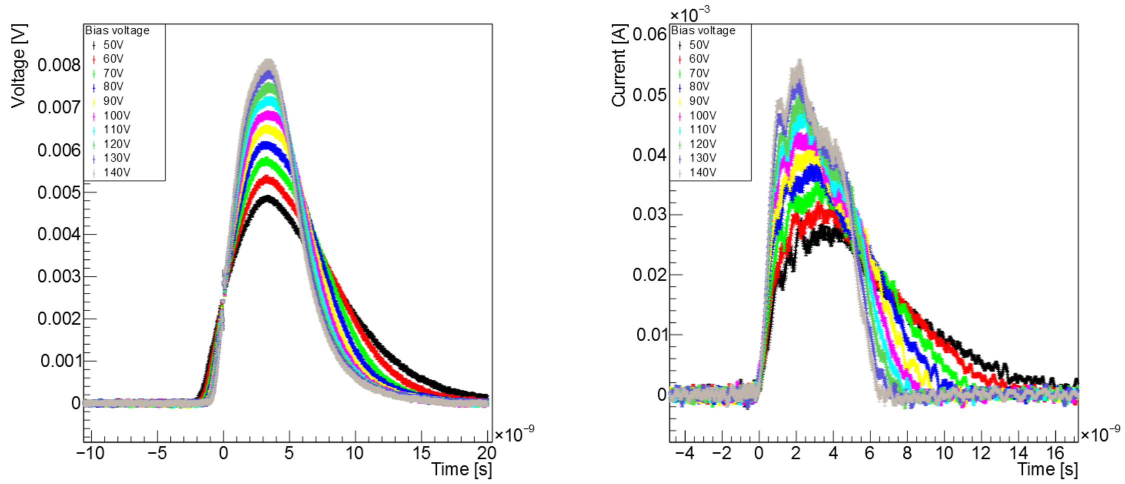

(a) TCT voltage signal.

(b) Shifted current.

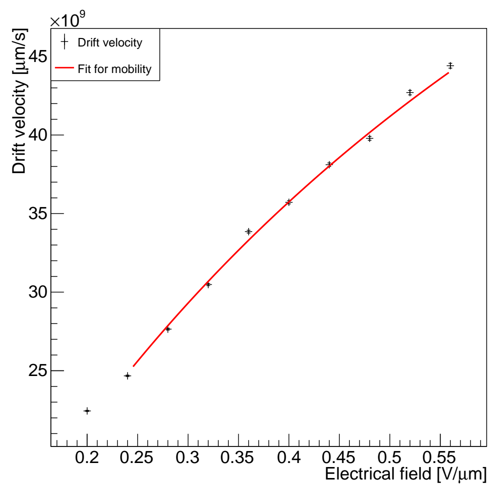

(c) Mobility fit.

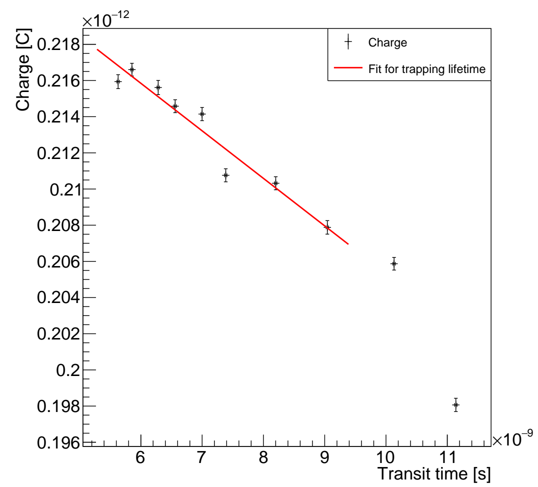

(d) Lifetime fit.

Figure A.3.: Data set 2.1.

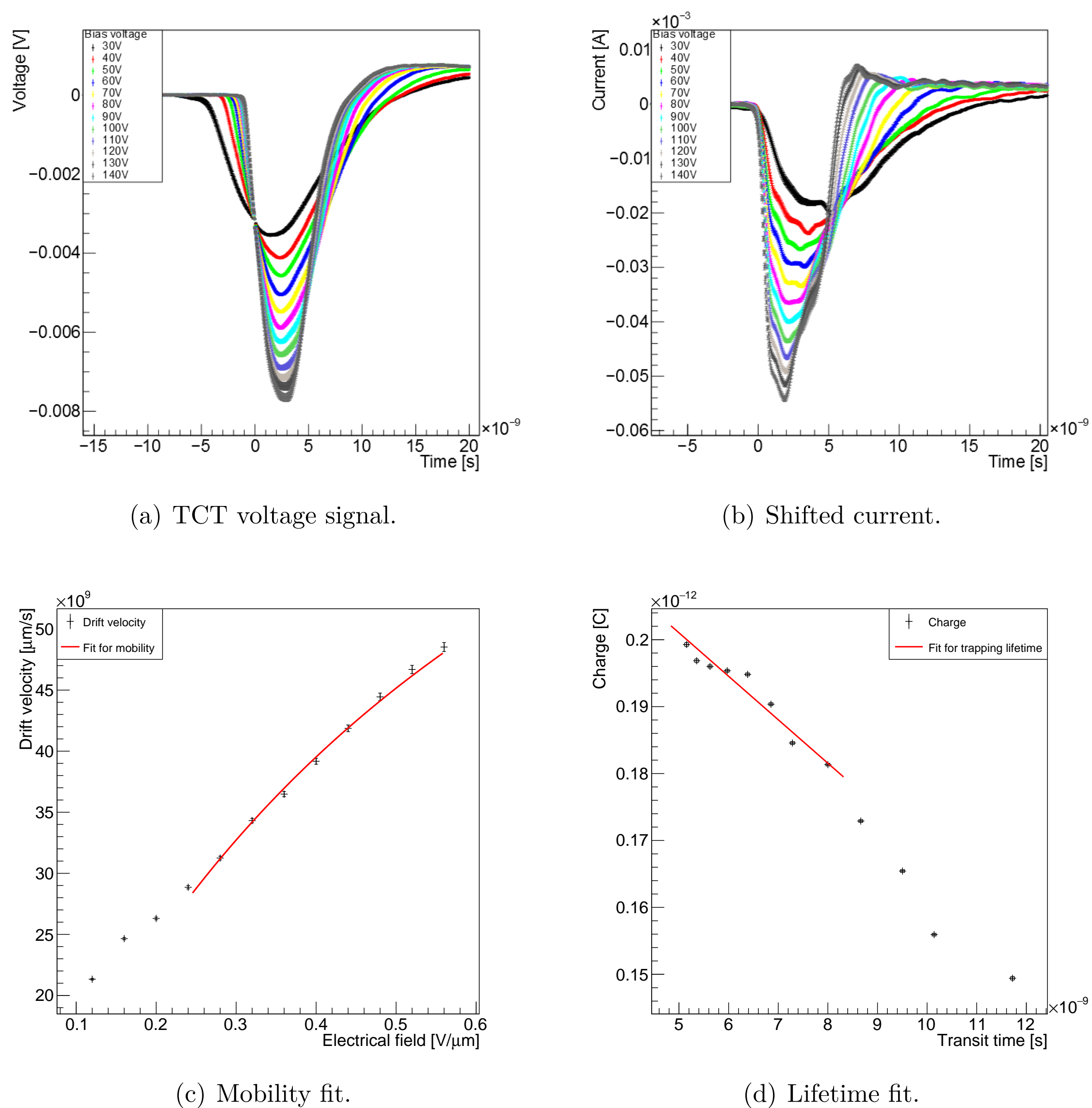

(a) TCT voltage signal.

(b) Shifted current.

(c) Mobility fit.

(d) Lifetime fit.

Figure A.4.: Data set 2.2.

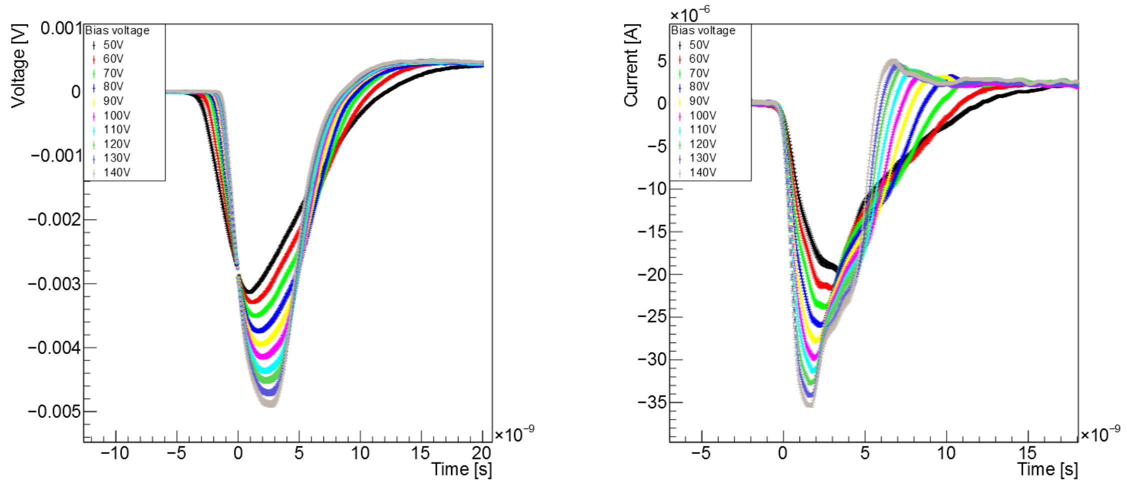

(a) TCT voltage signal.

(b) Shifted current.

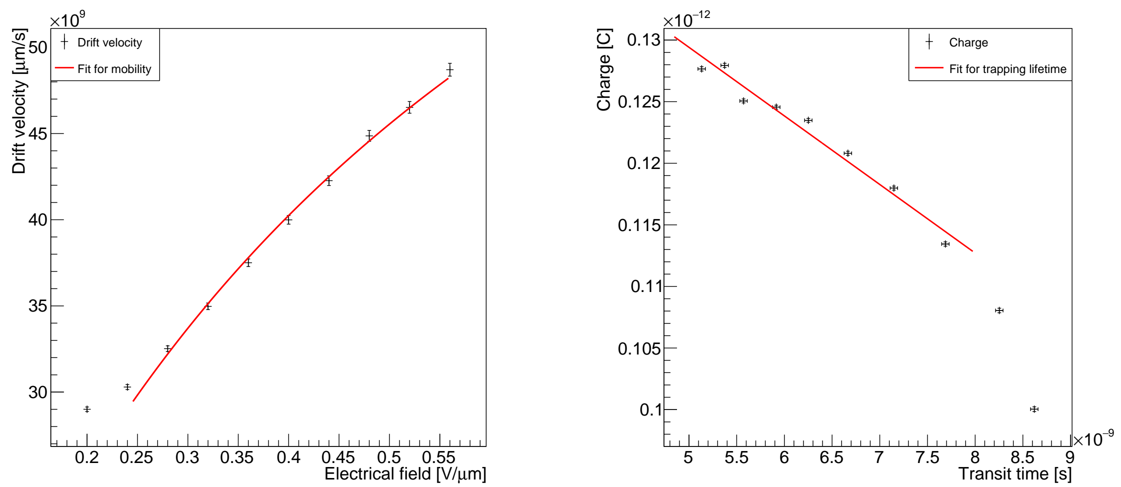

(c) Mobility fit.

(d) Lifetime fit.

Figure A.5.: Data set 2.3.

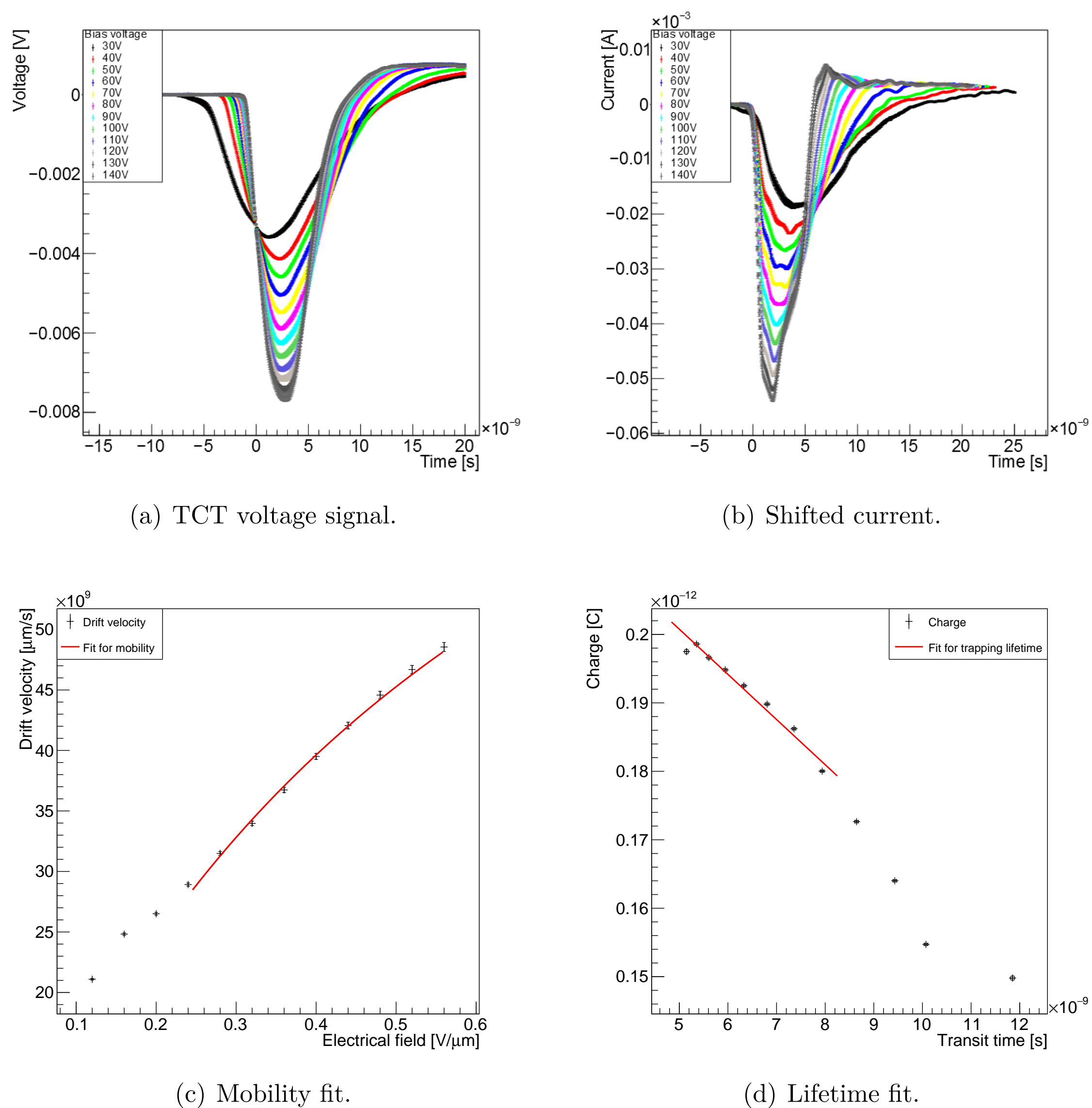

(a) TCT voltage signal. (b) Shifted current.

(c) Mobility fit. (d) Lifetime fit.

Figure A.6.: Data set 3.1.

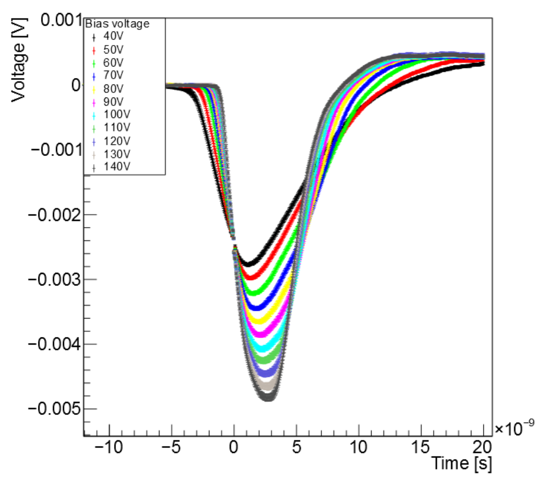

(a) TCT voltage signal.

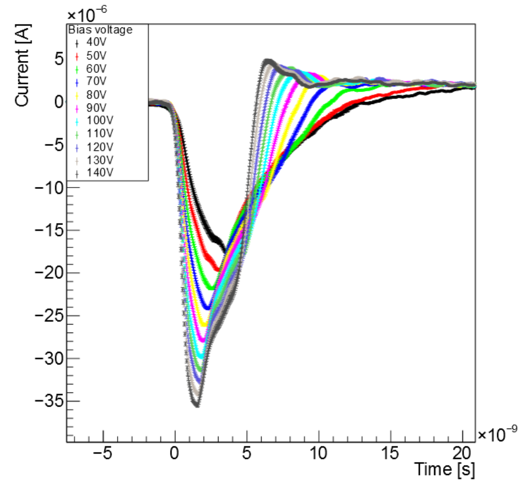

(b) Shifted current.

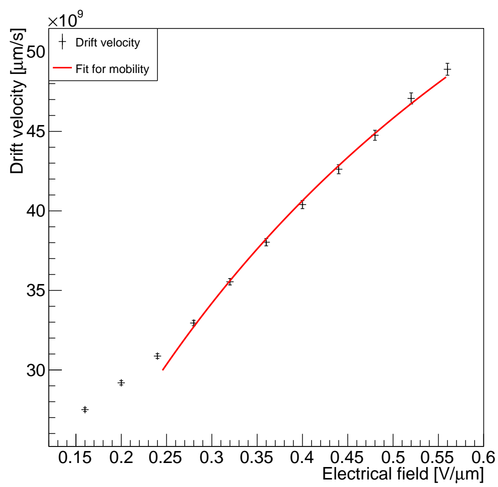

(c) Mobility fit.

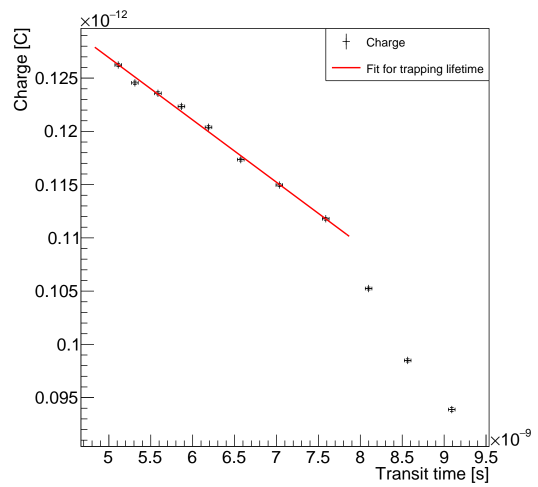

(d) Lifetime fit.

Figure A.7.: Data set 3.2.

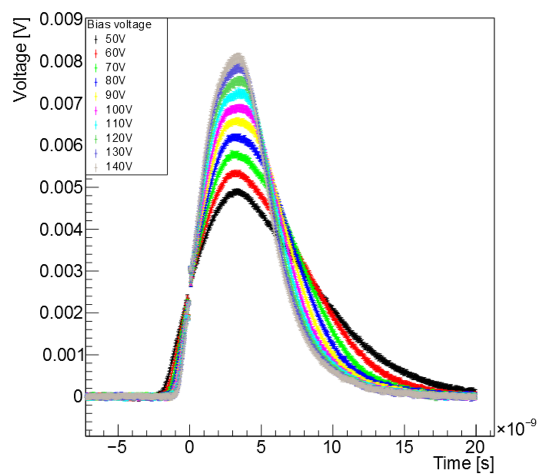

(a) TCT voltage signal.

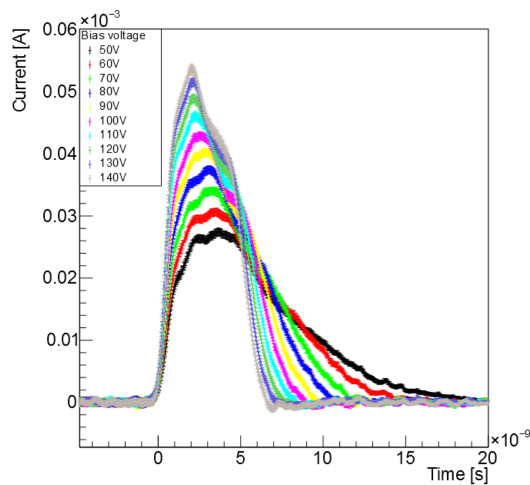

(b) Shifted current.

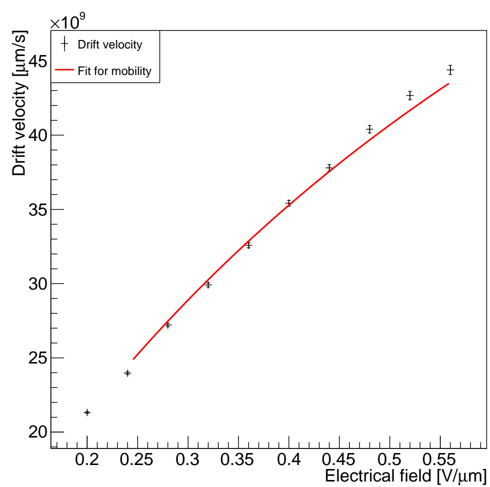

(c) Mobility fit.

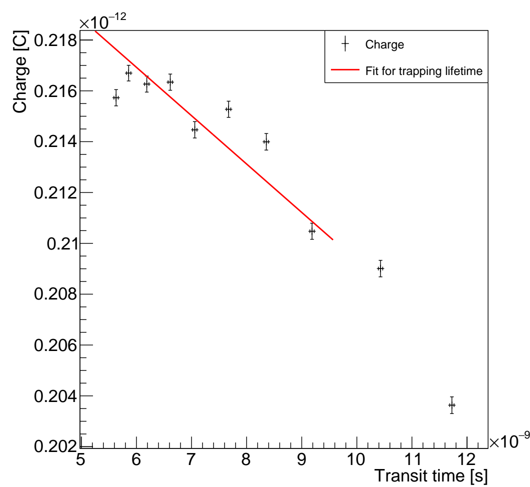

(d) Lifetime fit.

Figure A.8.: Data set 3.3.

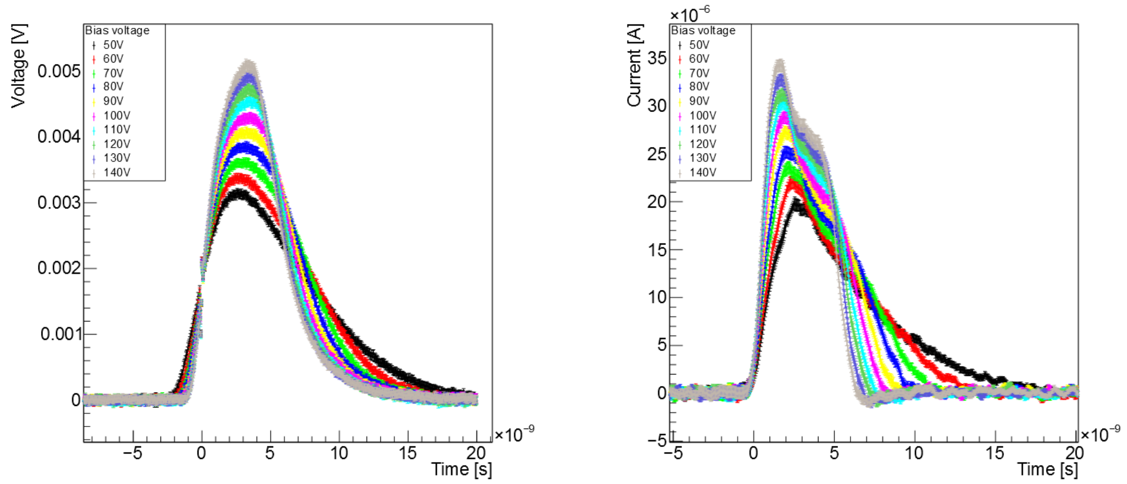

(a) TCT voltage signal.

(b) Shifted current.

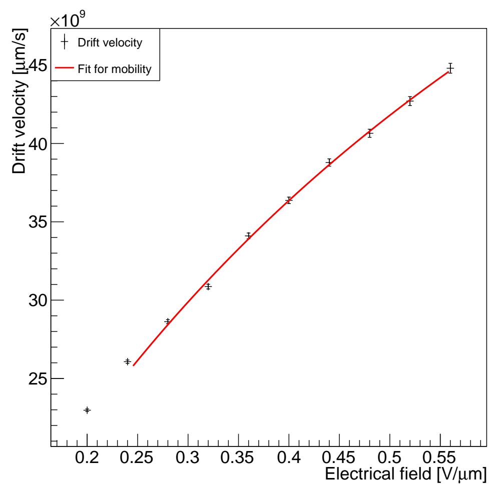

(c) Mobility fit.

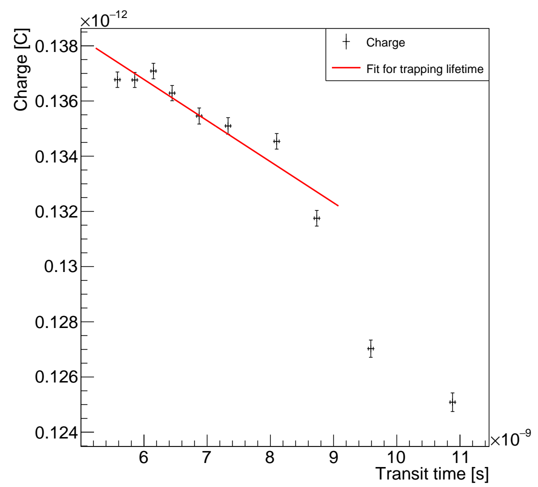

(d) Lifetime fit.

Figure A.9.: Data set 3.4.

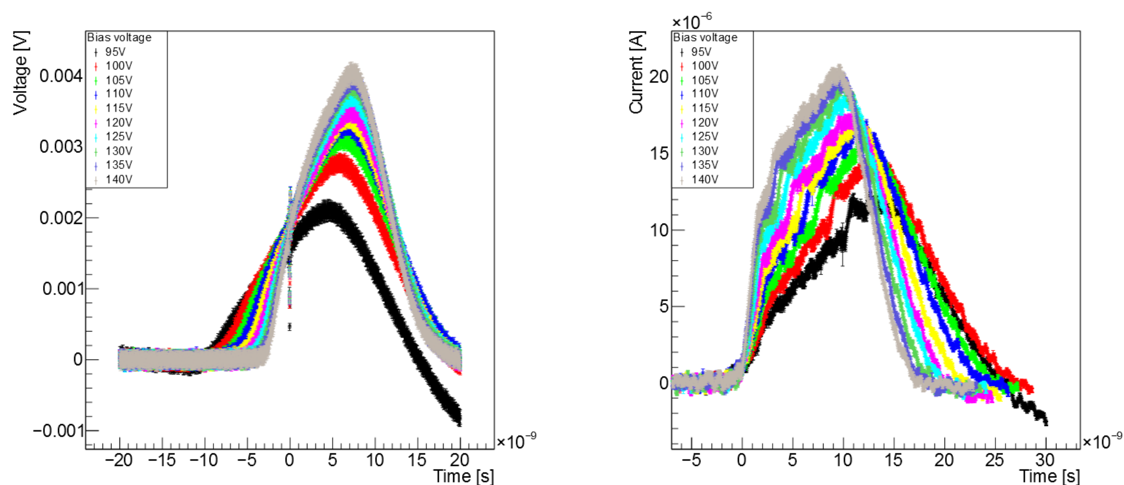

(a) TCT voltage signal.

(b) Shifted current.

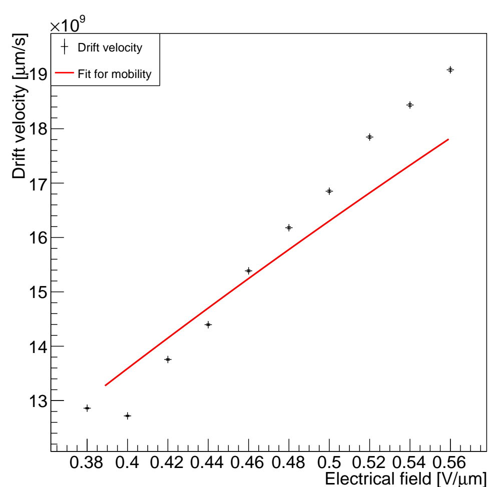

(c) Mobility fit.

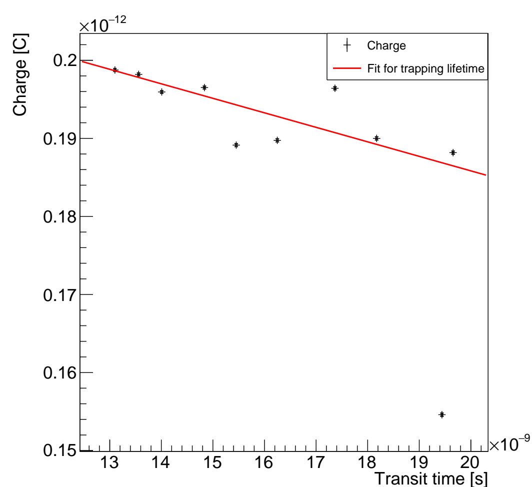

(d) Lifetime fit.

Figure A.10.: Data set 4.1.

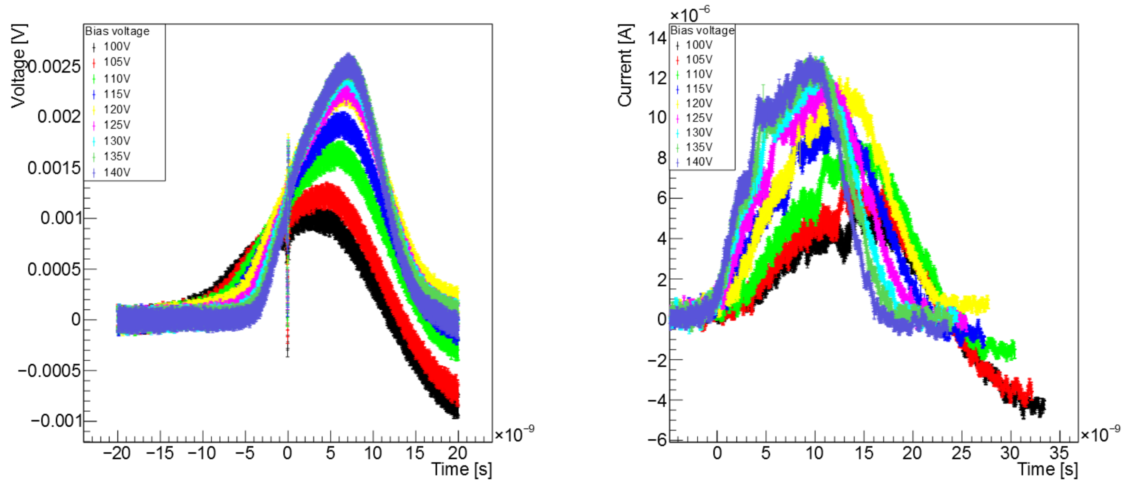

(a) TCT voltage signal.

(b) Shifted current.

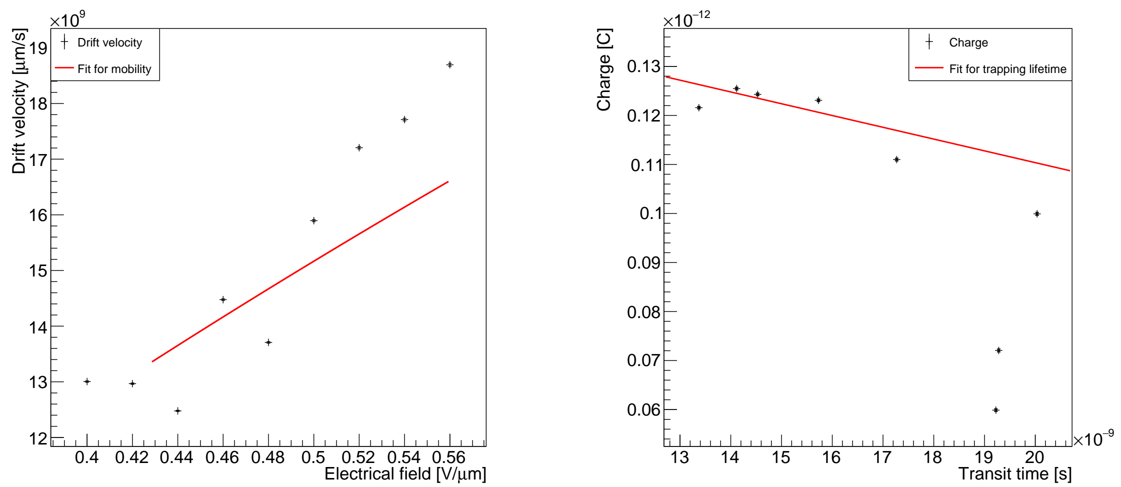

(c) Mobility fit.

(d) Lifetime fit.

Figure A.11.: Data set 4.2.

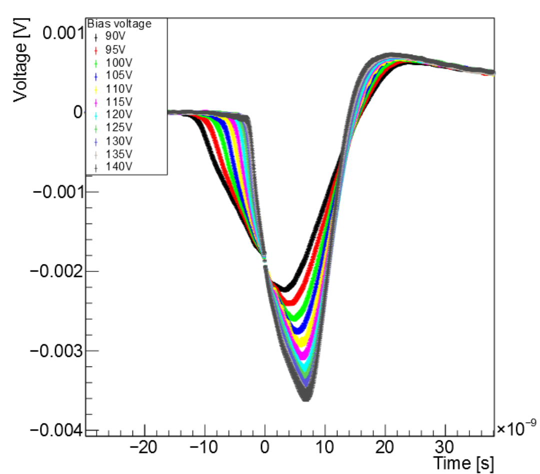

(a) TCT voltage signal.

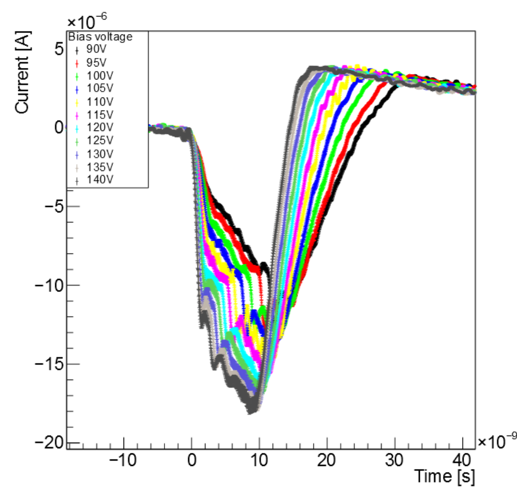

(b) Shifted current.

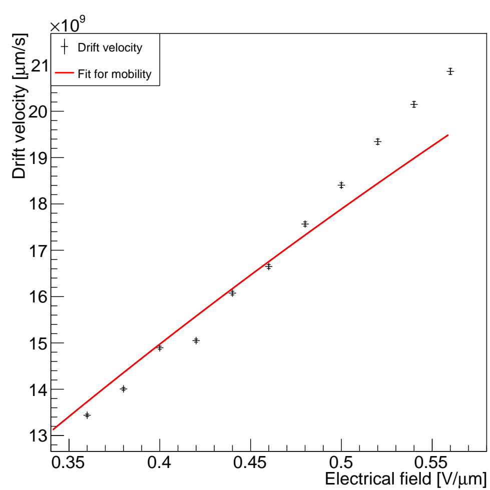

(c) Mobility fit.

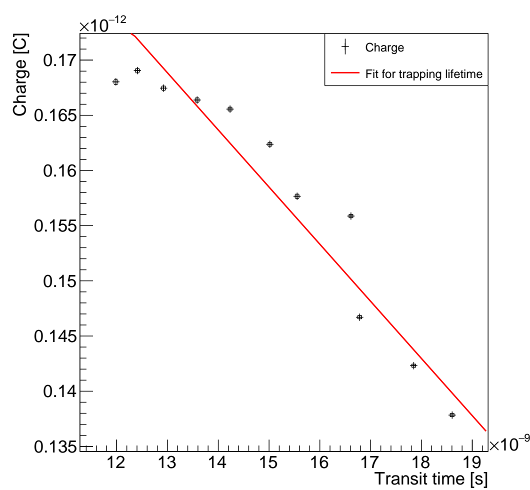

(d) Lifetime fit.

Figure A.12.: Data set 4.3.

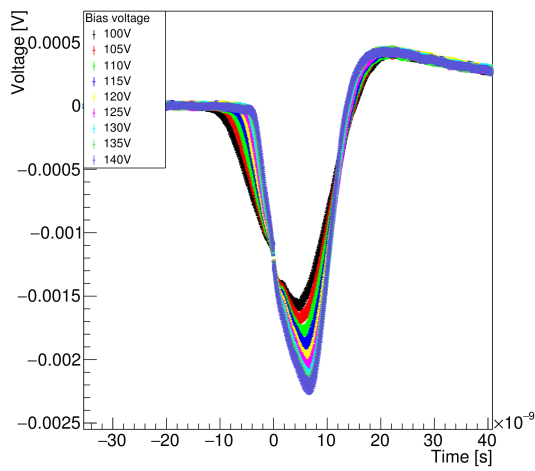

(a) TCT voltage signal.

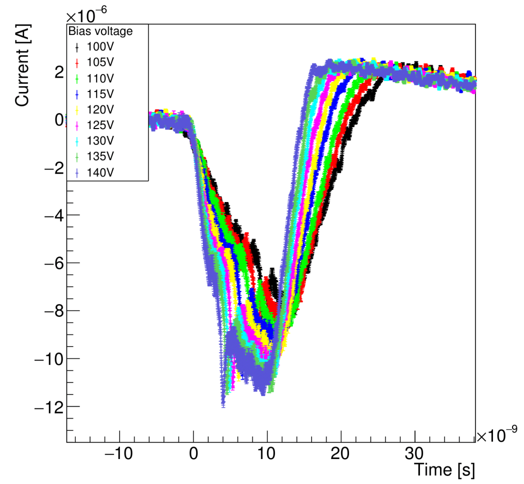

(b) Shifted current.

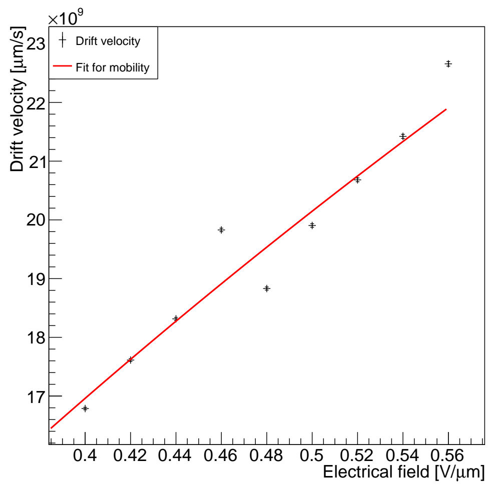

(c) Mobility fit.

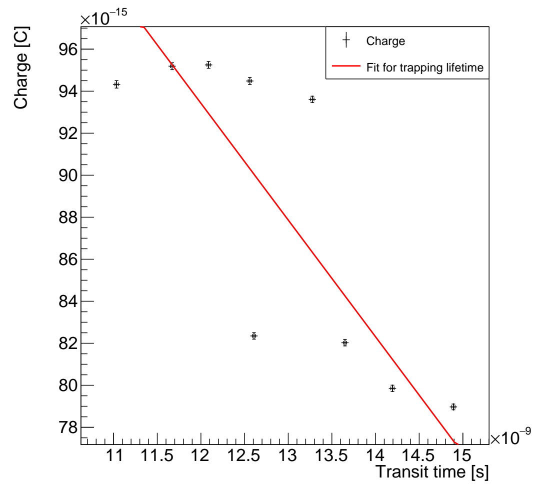

(d) Lifetime fit.

Figure A.13.: Data set 4.4.

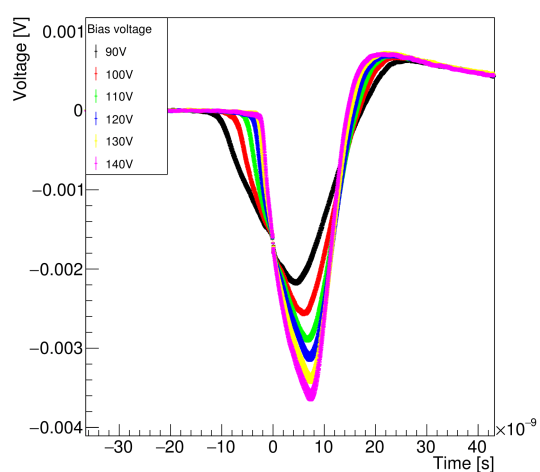

(a) TCT voltage signal.

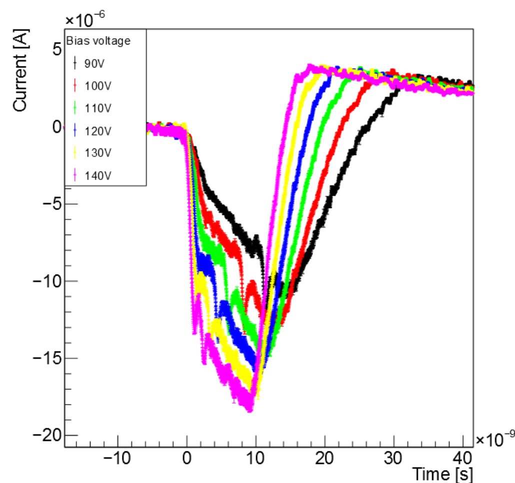

(b) Shifted current.

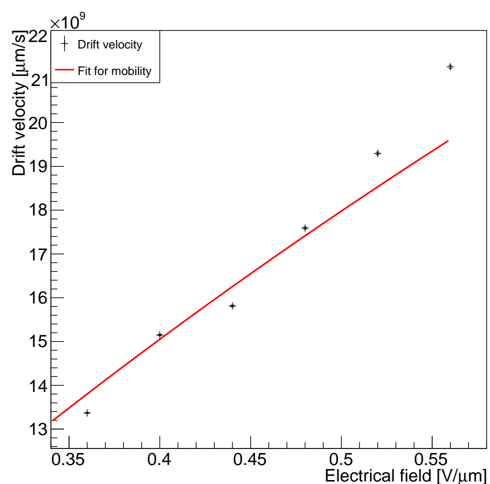

(c) Mobility fit.

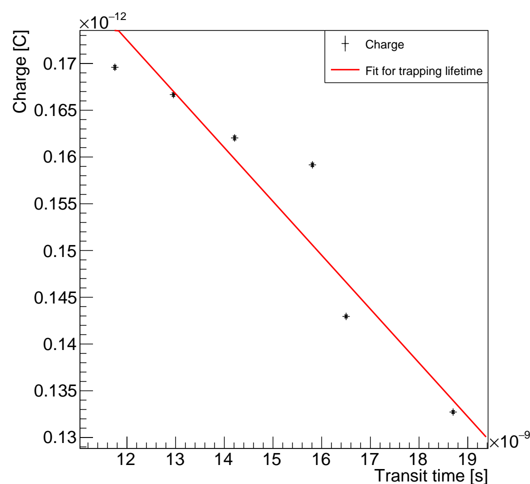

(d) Lifetime fit.

Figure A.14.: Data set 5.1.

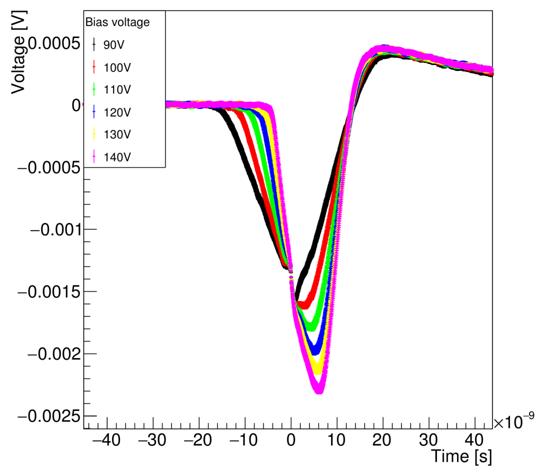

(a) TCT voltage signal.

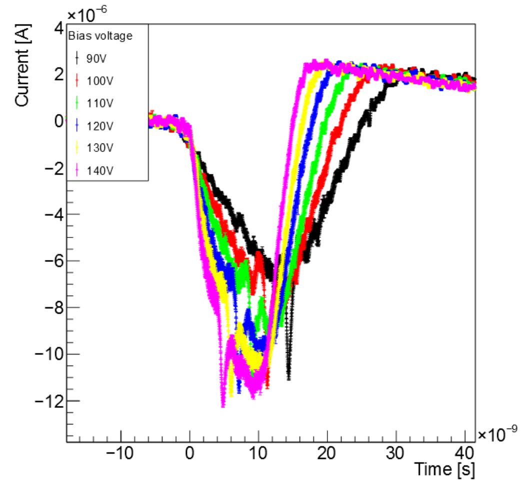

(b) Shifted current.

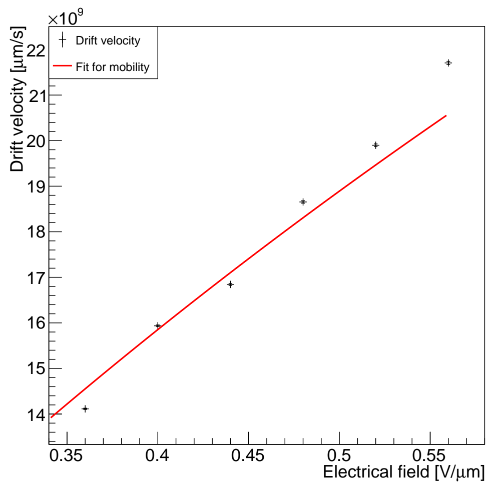

(c) Mobility fit.

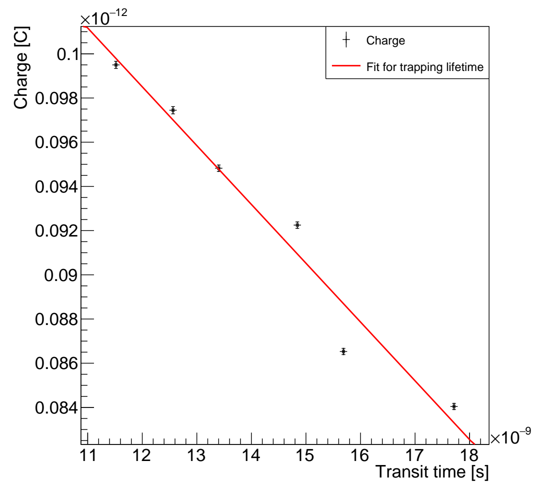

(d) Lifetime fit.

Figure A.15.: Data set 5.2.

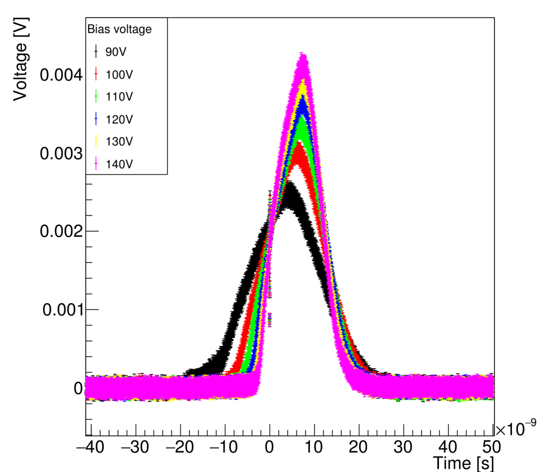

(a) TCT voltage signal.

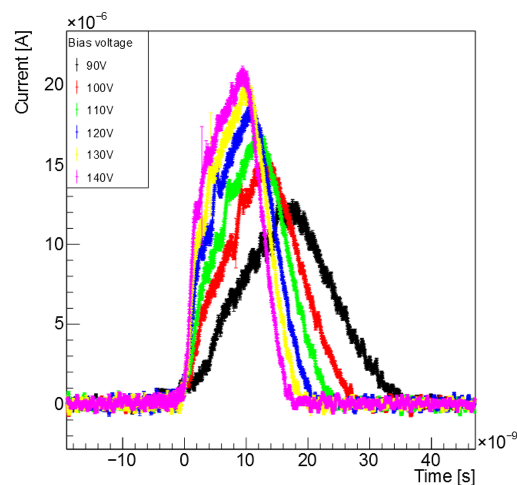

(b) Shifted current.

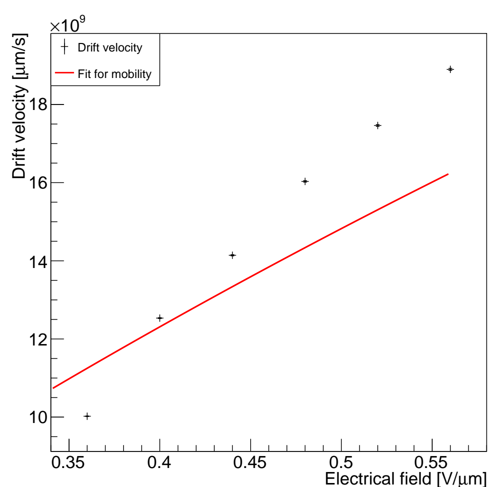

(c) Mobility fit.

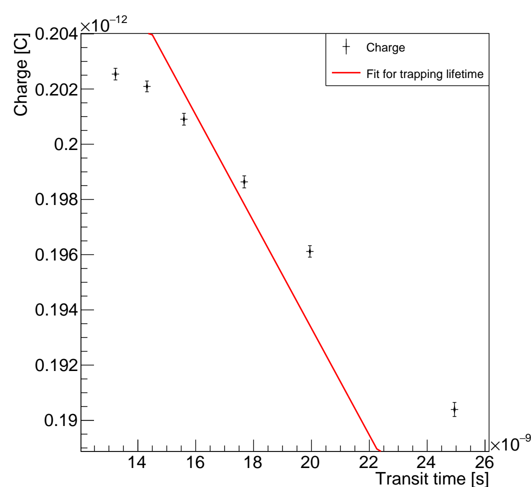

(d) Lifetime fit.

Figure A.16.: Data set 5.3.

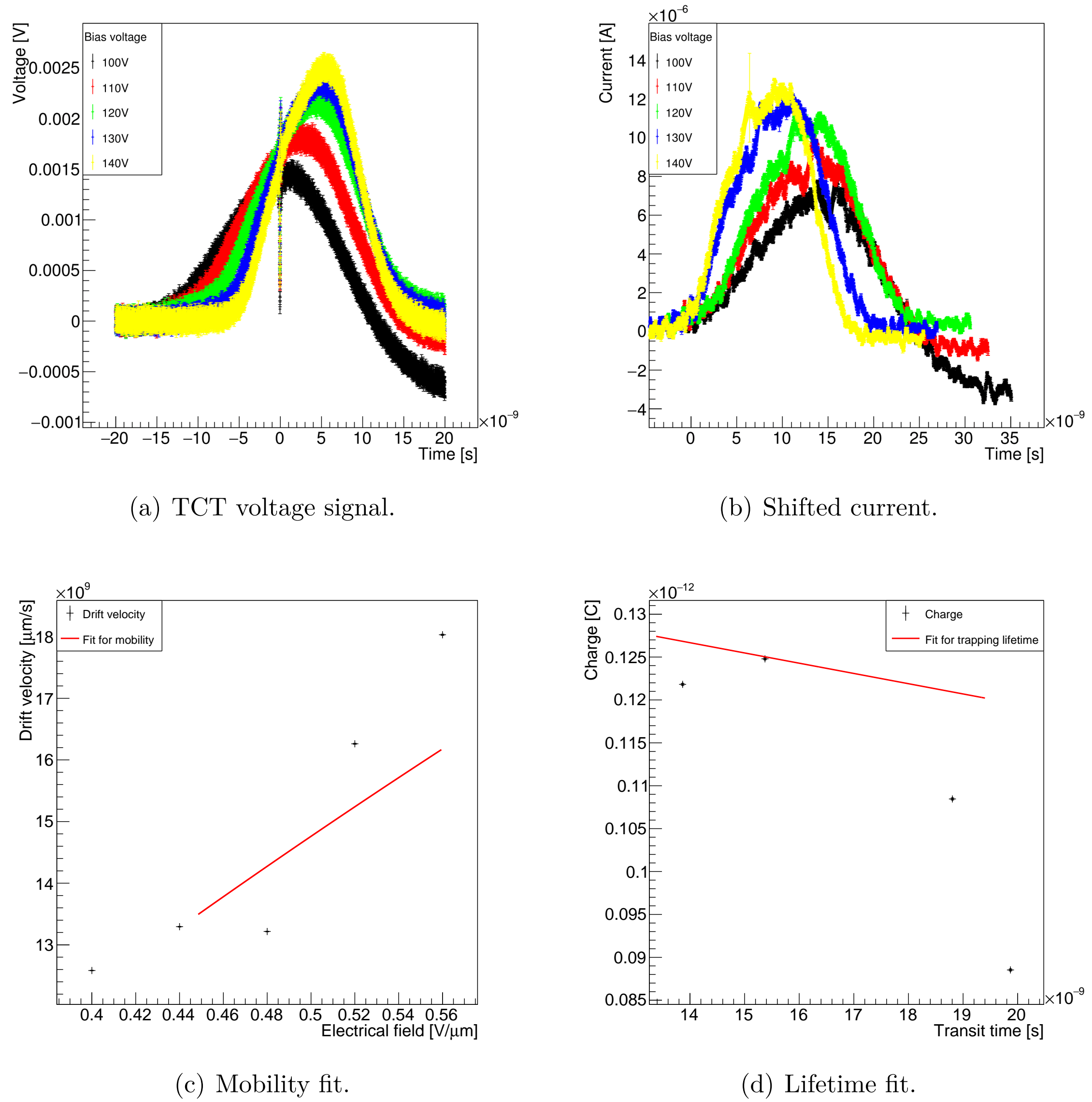

(a) TCT voltage signal.

(b) Shifted current.

(c) Mobility fit.

(d) Lifetime fit.

Figure A.17.: Data set 5.4.

A.2. Diamond

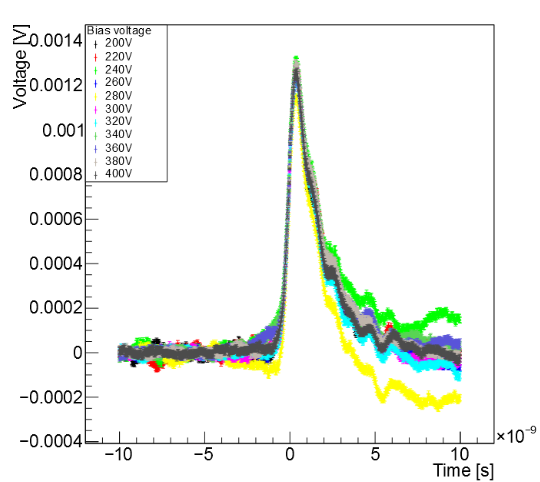

(a) TCT voltage signal.

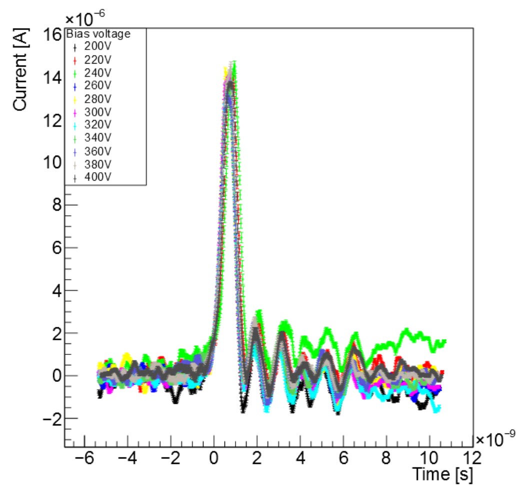

(b) Shifted current.

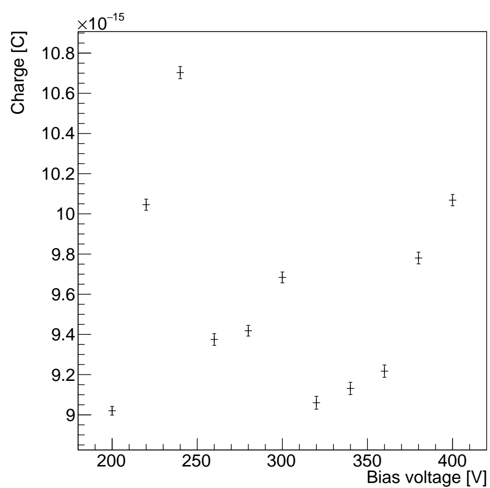

(c) Charge.

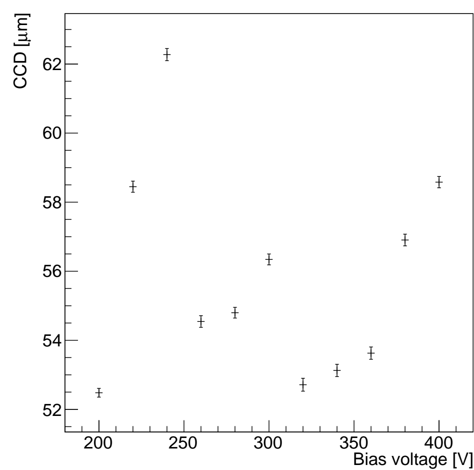

(d) CCD.

Figure A.18.: Data set 1.

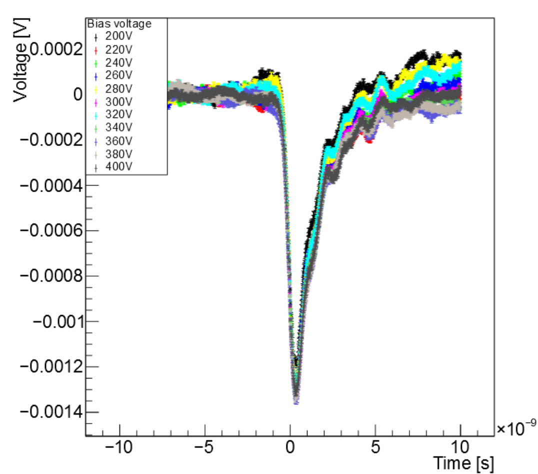

(a) TCT voltage signal.

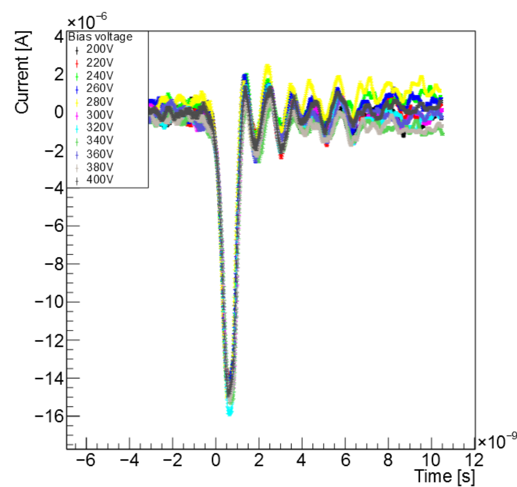

(b) Shifted current.

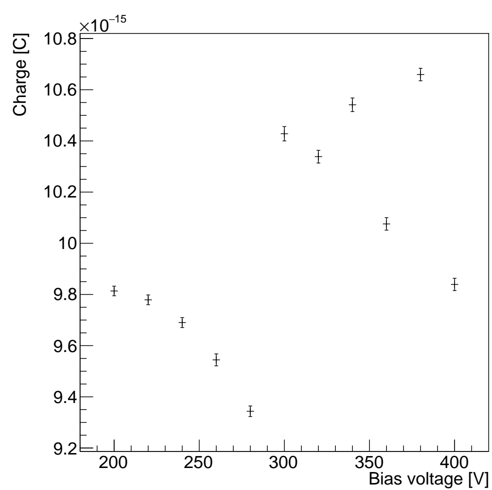

(c) Charge.

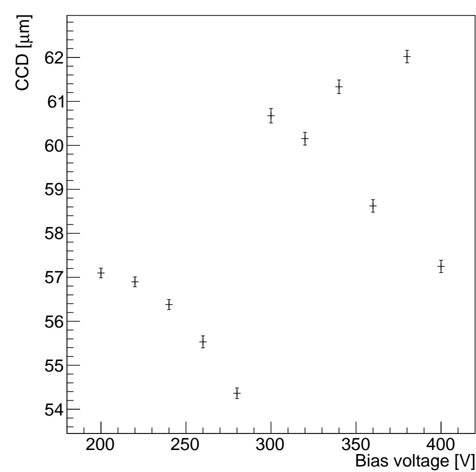

(d) CCD.

Figure A.19.: Data set 2.

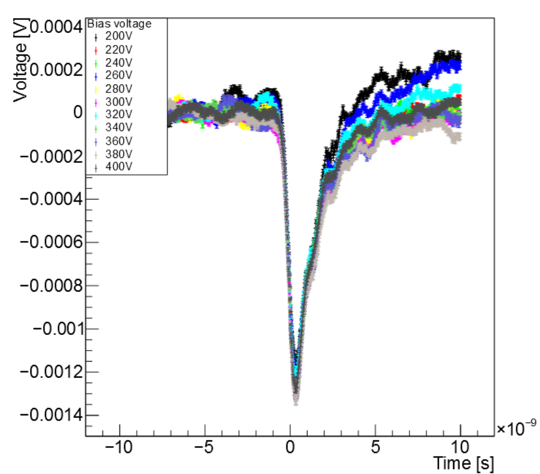

(a) TCT voltage signal.

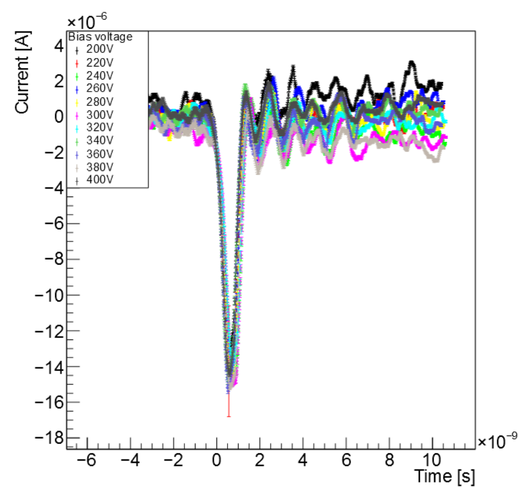

(b) Shifted current.

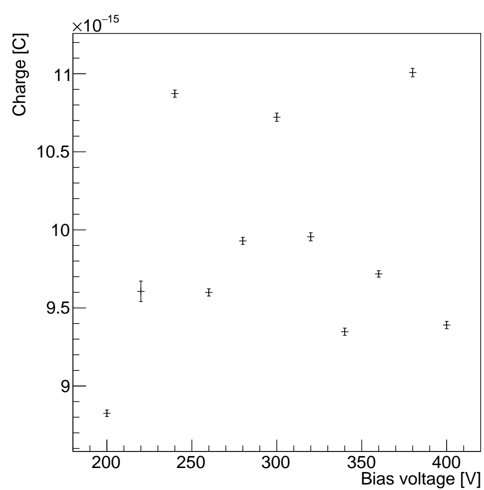

(c) Charge.

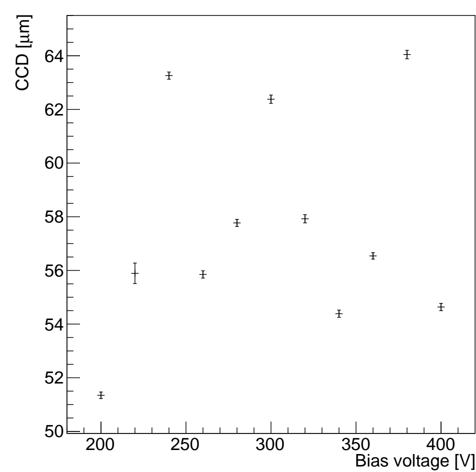

(d) CCD.

Figure A.20.: Data set 3.

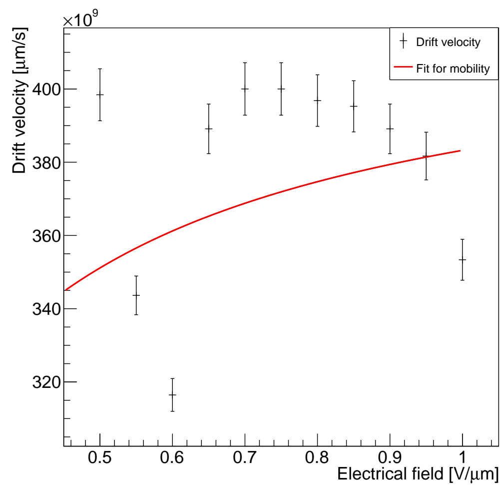

(a) Mobility fit.

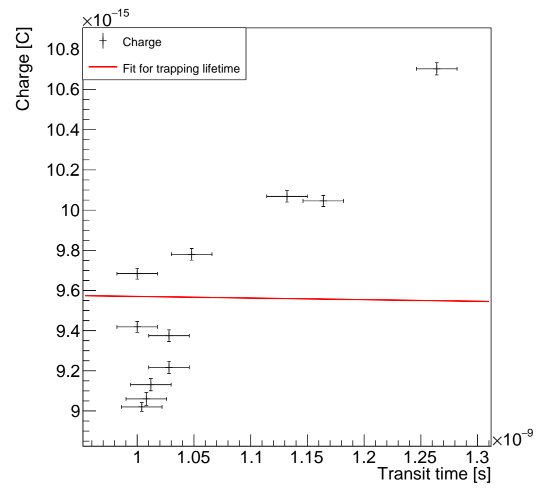

(b) Lifetime fit.

Figure A.21.: Data set 1.

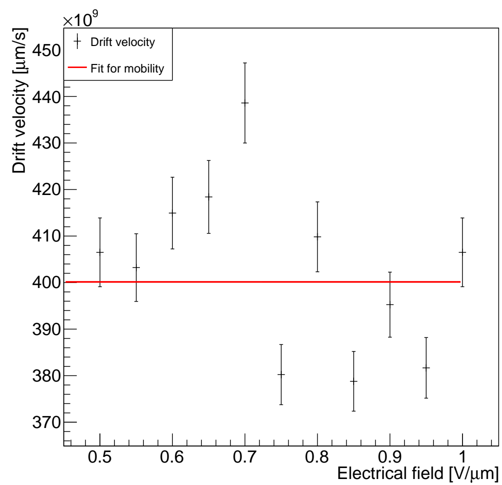

(a) Mobility fit.

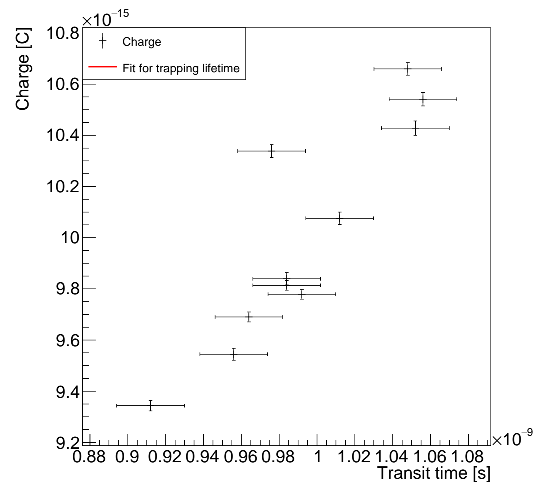

(b) Lifetime fit.

Figure A.22.: Data set 2.

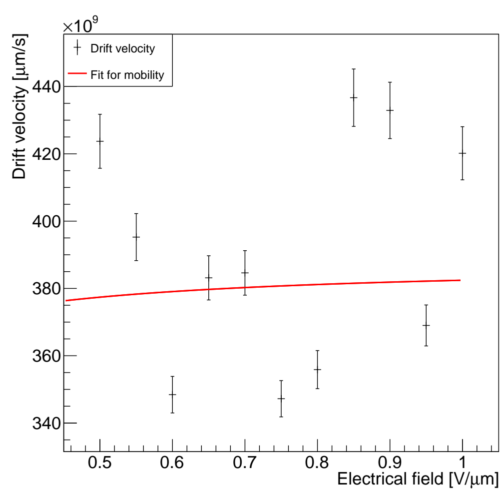

(a) Mobility fit.

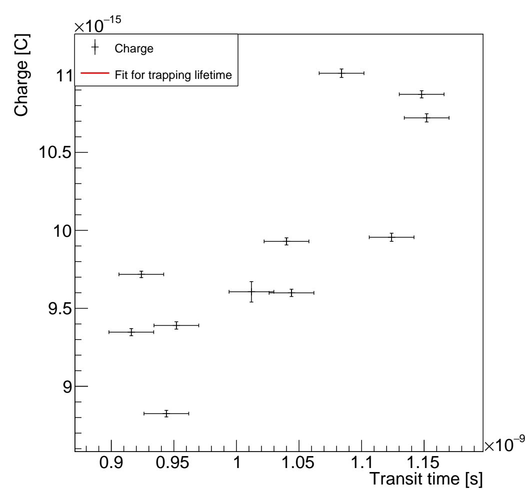

(b) Lifetime fit.

Figure A.23.: Data set 3.

Bibliography

[1] W. R. Leo, *Techniques for Nuclear and Particle Physics Experiments: A How-to Approach*, Springer-Verlag (1994)

[2] K. A. Olive et al. (Particle Data Group), *The Review of Particle Physics*, Chin. Phys. C **38**, 010009 (2014)

[3] David Casas et al., *Proton Stopping Power of Different Density Profile Plasmas* (2014), `arXiv:1409.6152[physics.plasm-ph]`

[4] I. Peric, *Active pixel sensors in high-voltage CMOS technologies for ATLAS*, Journal of Instrumentation **7(08)**, C08002 (2012)

[5] A. L. Schorlemmer, *Monitoring Radiation Damage in the ATLAS Pixel Detector*, Ph.D. thesis, Georg-August Universität Göttingen (2014)

[6] G. Kramberger, *Signal development in irradiated silicon detectors*, Ph.D. thesis, University Ljubljana (2001), CERN-Thesis-2001-038

[7] M. Capeans et al., *ATLAS Insertable B-Layer Technical Design Report*, Technical Report CERN-LHCC-2010-013. ATLAS-TDR-19, CERN, Geneva (2010)

[8] I. Friel, *Optical Engineering of Diamond*, chapter 2: Optical Quality Diamond Grown by Chemical Vapor Deposition, WILEY-VCH (2013)

[9] F. P. Bundy et al., *Man-made diamonds*, Nature **176**, 51 (1955)

[10] Y. Zhang et al., *Grain Boundary Structure and Growth Sequence of Diamond Thin Film*, Materials Science Forum **204-206**, 207 (1996)

[11] D. Asner et al., *Diamond pixel modules*, Nucl. Instr. and Meth. A **636(1, Supplement)**, 125 (2011), 7th International Hiroshima Symposium on the Development and Application of Semiconductor Tracking Detectors

[12] H. Pernegger, *High Mobility Diamonds and Particle Detectors*, WILEY-VCH (2008)

[13] H. Pernegger et al., *Charge-carrier properties in synthetic single-crystal diamond measured with the transient-current technique*, Journal of Applied Physics **97(7)**, 073704 (2005)

[14] S. Uxa et al., *Determination of Electric-Field Profile in CdTe and CdZnTe Detectors Using Transient-Current Technique*, IEEE Transactions on Nuclear Science **59(5)**, 2402 (2012)

[15] W. Shockley, *Currents to Conductors Induced by a Moving Point Charge*, Journal of Applied Physics **9(10)**, 635 (1938)

[16] S. Ramo, *Currents Induced by Electron Motion*, Proceedings of the IRE **27(9)**, 584 (1939)

[17] G. Kramberger, *Signal development in irradiated silicon detectors*

[18] C. Klein, *Development of a TCT Measurement Setup for Sensor Materials for Tracking Detectors in High-Energy Physics*, Master's thesis, University Göttingen, Göttingen (2014), II. Physik-UniGö-MSc-2014/09

[19] Kolter Eelectronic, *VV1000-LC3E linear preamplifier - Data Sheet* (2015)

[20] L. Graber, *Characterisation of highly irradiated polycrystalline diamond sensors for ionising radiation*, Master's thesis, University Göttingen, Göttingen (2011), II. Physik-UniGö-MSc-2011/01

[21] C. Canali et al., *Electron and hole drift velocity measurements in silicon and their empirical relation to electric field and temperature*, Electron Devices, IEEE Transactions on **22(11)**, 1045 (1975)

[22] D. Meier, *CVD Diamond Sensors for Particle Detection and Tracking*, Ph.D. thesis, Heidelberg University. (1999)

Danksagung

Ich danke Prof. Dr. Arnulf Quadt, dass er mir ermöglicht hat, diese Arbeit in seiner Arbeitsgruppe zu schreiben und mich mit Ratschlägen unterstützt hat. Mein Dank gilt auch der gesamten Gruppe für das gute Arbeitsklima. Besonders unterstützt haben mich dabei Dr. Jens Weingarten und Lars Graber. Für technische und praktische Hilfe danke ich der Elektronik- und der Feinmechanik-Werkstatt.

Dafür dass sie mir mein Studium ermöglicht haben und mir in allen Lagen geholfen haben, kann ich mich nicht genug bei meinen Eltern bedanken.

Erklärung nach §18(8) der Prüfungsordnung für den Bachelor-Studiengang Physik und den Master-Studiengang Physik an der Universität Göttingen:

Hiermit erkläre ich, dass ich diese Abschlussarbeit selbständig verfasst habe, keine anderen als die angegebenen Quellen und Hilfsmittel benutzt habe und alle Stellen, die wörtlich oder sinngemäß aus veröffentlichten Schriften entnommen wurden, als solche kenntlich gemacht habe.
Darüberhinaus erkläre ich, dass diese Abschlussarbeit nicht, auch nicht auszugsweise, im Rahmen einer nichtbestandenen Prüfung an dieser oder einer anderen Hochschule eingereicht wurde.

Göttingen, den June 2, 2017

(Helge Christoph Beck)